

Received 10 May 2023, accepted 7 July 2023, date of publication 17 July 2023, date of current version 21 July 2023.

Digital Object Identifier 10.1109/ACCESS.2023.3296256

RESEARCH ARTICLE

Low-Complexity PAPR Reduction by Coded Data Insertion on DVB-T2 Reserved Carriers

GIUSEPPE BARUFFA¹, LUCA RUGINI¹, (Member, IEEE), FABRIZIO FRESCURA¹,
AND PAOLO BANELLI¹, (Member, IEEE)

Department of Engineering, University of Perugia, 06125 Perugia, Italy

Corresponding author: Giuseppe Baruffa (giuseppe.baruffa@unipg.it)

This work was supported in part by the Fondo di Ricerca di Base 2022 Project “Energy-Efficient Networking, Signal Processing and Communications (EFESO)” funded by the University of Perugia; in part by the Fondo di Ricerca di Base 2020 Project “Systems, Algorithms, and Architectures for Information Transmission and Processing in Future Telecommunications and Sensor Networks” funded by the University of Perugia; and in part by the “Liquid Edge Computing Based on Distributed Machine Learning and Millimeter-Wave Radio Access (LIQUID_EDGE)” funded by the Ministero dell’Istruzione, dell’Università e della Ricerca (MIUR) under Project PRIN 2017.

ABSTRACT Digital terrestrial video broadcasting systems based on orthogonal frequency division multiplexing (OFDM), such as the second generation of terrestrial digital video broadcasting standard (DVB-T2), often include carriers reserved for peak-to-average power ratio (PAPR) reduction. This paper presents a low-complexity PAPR reduction method that inserts coded data onto a subset of reserved carriers. Using differential binary phase shift keying (DBPSK) with repetition coding, the proposed method generates a time-domain peak-cancellation signal that carries also additional information. The carrier selection, as well as the signal amplitudes, of the coded DBPSK data is optimized, taking also under control the regrowth of other peaks. Simulation results show that the proposed algorithm outperforms the tone reservation (TR) algorithm of the DVB-T2 standard in terms of both PAPR reduction performance and computational complexity. The proposed algorithm is also significantly less complex than the clipping-and-filtering (CF) algorithm and the active constellation extension (ACE) algorithm of the DVB-T2 standard, paying a small price in terms of PAPR. Noteworthy, the compatibility with existing DVB-T2 receivers is fully guaranteed, since the proposed method modifies only the reserved carriers.

INDEX TERMS DVB-T2, PAPR reduction, tone reservation, peak cancellation.

I. INTRODUCTION

Digital terrestrial television systems such as those standardized by the Digital Video Broadcasting (DVB) Consortium, the Advanced Television Systems Committee (ATSC), and the Digital Broadcasting Experts Group (DiBEG), have been designed to deliver high definition video [1], [2], [3]. The physical layers of DVB-terrestrial (DVB-T), second generation DVB-T (DVB-T2) [4], ATSC, ATSC 3.0, ISDB-terrestrial (ISDB-T), and ISDB-T Brazil (ISDB-Tb) are based upon coded orthogonal frequency-division multiplexing (OFDM), which can deal with communication channels impaired by multipath, fading, and non line-of-sight (NLOS) conditions. However, one of the main

problems of OFDM, at the transmission side, is the high peak to average power ratio (PAPR) generated by the possibility that several OFDM carriers may add in-phase in the time domain [5]. Thus, differently from constant-envelope single-carrier modulations, characterized by a low PAPR, multicarrier modulations like OFDM suffer from high PAPR, especially when there are thousands of carriers. Unfortunately, signals with large PAPR lead to a reduced efficiency of the power amplifier and, definitely, to a waste of electrical power [6].

In the last two decades, several solutions for PAPR reduction have been proposed in the literature. A survey of different PAPR reduction methods can be found in [6] and [7]. For the sake of brevity, in this introduction, we briefly mention the main methods, with their advantages and drawbacks, including some recent techniques. Among

The associate editor coordinating the review of this manuscript and approving it for publication was Yunlong Cai¹.

low-complexity methods, clipping-and-filtering (CF) [8] is an effective approach in reducing the PAPR, at the price of significant in-band distortions that deteriorate the bit error rate (BER) performance [6]. Using optimized CF, PAPR reduction may be improved at the expense of increased complexity [9], [10] or side information [11]. Nonlinear companding [12], [13], [14], [15], [16], [17], [18] has low complexity, but, similarly to clipping, in-band distortions are introduced. Also near-complementary sequences can be used to reduce the PAPR [19], as well as optimized waveform design [20], [21], [22]. More complex methods, such as channel coding [6], [23], [24], [25], discrete Fourier transform (DFT) precoding [26], [27], other transform coding [28], rotated constellations [29], index modulation with dithering [30], deep learning [31], and genetic algorithms [32] can be used to reduce the PAPR, but these methods have a detrimental effect on the data rate or on the complexity. Some other methods require the transmission of side information together with the original data, which makes them unsuitable for the broadcasting standards already in use [33], [34]. For instance, the partial transmit sequence (PTS) technique splits the signal in distinct blocks, which are then recombined together with optimal phase offsets, to reduce the PAPR [35], [36], [37], [38]. Clearly, in this case, both the segmentation strategy and the phase offsets must be known at the receiver to reconstruct the original signal [39]. Differently, the selective mapping (SLM) technique requires the transmitters to generate several different versions of the data signal, each one multiplied by a random phase offset sequence: the version with the smallest PAPR is selected for transmission [40], [41]. Even in this case, the optimal phase sequence must be communicated to the receiver. In addition, some other techniques optimize the position of null or free carriers [42], [43]: this is not suitable for DVB-T2, where the position of reserved carriers is predetermined by the standard [4].

Other methods, such as tone reservation (TR) and active constellation extension (ACE), do not require side information transmission. TR adopts a reserved set of OFDM carriers, unused for data transport, which are utilized to actively reduce signal peaks by proper modulation [44], [45], [46], [47], [48], [49], [50], [51], [52], [53], [54], [55], [56], [57], [58], [59].

The TR approach has been formulated as a convex linear programming (LP) problem, whose closed-form solution, as well as a simplified algorithm based on gradient descent, was proposed by Tellado [44]. Among the different variants of TR PAPR reduction methods that have been proposed, a first set is based on splitting the reserved carriers into different groups. For instance, Mroué et al. [45] control the power of each group, so as to cancel multiple peaks at each iteration. Bulusu et al. [46] also use multiple groups, with minimization of many peaks at each iteration. In addition, Lahbabi et al. [47] employ a group-wise TR to limit also complexity and latency, by simplifying the peak search and optimizing the inserted signal phases.

A second set of variants of TR methods makes use of approximations or iterative methods to reduce complexity. For instance, Li et al. [48] determine the peak canceling signal through a least-squares approximation of the original clipping noise. On the other hand, Wang et al. [49] adopt a fast iterative shrinkage-thresholding algorithm (FISTA) based on proximal maps, which has reduced complexity with respect to the original convex LP problem. Moreover, El Hassan et al. derive novel theoretical expressions for the error vector magnitude (EVM) of a PAPR-reduced OFDM signal, when TR with either gradient descent [50] or quadratic programming [51], [52] is applied. With a similar approach, Liu et al. [53] apply the alternate direction method of multipliers (ADMM) to the convex LP TR method, so as to relieve some of its complexity.

In addition to the variants previously listed, other TR-based PAPR reduction algorithms have been proposed. One example is the one of Mounzer et al. [54], which expands the TR method of DVB-T2 by adding more control on the power constraint and on the selected threshold. As another example, Jiang et al. [55] adopt a multiblock TR method to combat PAPR in multicarrier systems based on overlapping and filtered data blocks. Differently, Zayani et al. [56] combine TR optimization and digital predistortion steps together in an iterative manner, so as to obtain a synergistic improvement on emitted signal linearity. Instead, Nguyen et al. [57] propose two different algorithms based on TR, where a step is precomputed offline, and another step is applied in real-time to the OFDM signal in a wireline scenario. Shehata et al. [58] use some TR methods to reduce the PAPR of compressed OFDM signals in cloud-based radio access network, opening a new application field for TR and CF methods. PAPR reduction by TR optimization is proposed also for MIMO-OFDM radar processing, for example by Wu et al. in [59].

A limiting factor of the TR methods is the reduced number of available reserved carriers in existing systems: in order to maintain a backward compatibility, the PAPR performance of TR methods is somewhat limited by the number of reserved carriers. On the other hand, ACE [60], [61], [62], [63] acts on the quadrature amplitude modulation (QAM) of data carriers and modifies some selected edge points of the QAM constellation by extending them outwards: this offset does not degrade the BER performance at the receiver, but reduces the peak amplitudes at the transmitter. Both TR and ACE are included in DVB-T2 and ATSC 3.0, but their complexity can be relevant [4], [6], [60], [64], [65], especially for ACE methods that modify thousands of data carriers. Hybrid schemes are also possible, such as for instance [66], which uses CF with companding, [67], which combines SLM with ACE, [68], mixing TR and CF, and [69], which adopts SLM, PTS, and companding. Finally, there are also hardware-based methods, such as those using a bank of amplifiers in parallel [70].

A common feature of most PAPR reduction methods is their focus on performance improvement, with secondary goal of complexity reduction. A main motivation of our

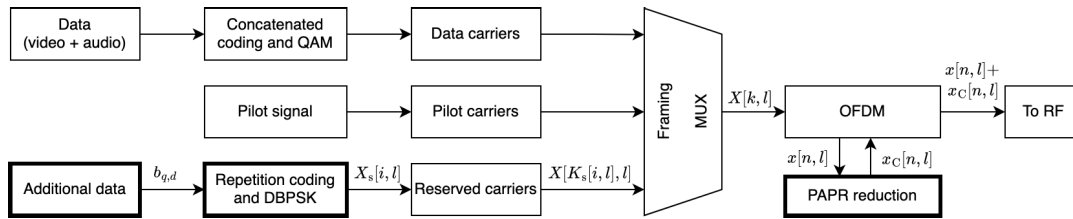


FIGURE 1. System model of the considered DVB-T2 transmitter. The proposed features are in the three blocks with thick lines.

work is to give equal importance to both performance and complexity. We aim at PAPR reduction, with limited complexity as a necessary goal. Specifically, this paper proposes a low-complexity TR-like PAPR reduction method for the DVB-T2 standard [4]. From the complexity viewpoint, our proposal is notably cheaper than conventional TR and ACE of DVB-T2, and than CF. Moreover, ACE cannot be used with other DVB-T2 features, such as rotated constellations or Alamouti's coding [4], and can produce inaccurate calculation of log-likelihood ratios of the data bits [71].

To be more specific, the proposed method conveniently modulates a selected subset of the reserved carriers to reduce the largest peaks of the time-domain OFDM signal, while avoiding the regrowth of other peaks. Since the proposed method only modifies the reserved carriers, the error performance of the QAM data is almost unchanged, except for a 0.1 dB reduction of the data signal-to-noise ratio (SNR). In addition, the proposed method inserts a coded signal information into the reserved carriers, similarly to the transmission parameter signaling (TPS) used in DVB-T. The additional information could be useful for additional signaling, like additional parameters of transmission, additional bits for future extensions, watermarking, and other purposes. Approaches such as SLM and PTS allow for dramatic improvements in terms of PAPR attenuation, however this comes at the expense of a reduced spectral efficiency [6]. The proposed method, instead, offers a greater flexibility, since not only PAPR is reduced, but also additional data are included with respect to the DVB-T2 TR method. This additional data stream can be used for signaling and it is designed aiming at low BER, even after modification for PAPR reduction purposes. Simulation results show that the proposed method effectively reduces the PAPR of DVB-T2 signals, with better PAPR than for the conventional TR technique of the DVB-T2 standard [4].

In summary, the main contributions of this work are:

- A novel PAPR reduction method that, with respect to conventional TR, makes use of additional coded DBPSK data inserted in the reserved carriers while keeping backward-compatibility with existing DVB-T2 receivers;
- A low-complexity algorithm for carrier selection and weighting optimization, by projecting the coded DBPSK signal onto the QAM data signal to reduce the peaks;

- The derivation of a closed-form BER expression for the coded DBPSK data, validated by simulations;
- A performance-complexity comparison with some representative PAPR reduction strategies for DVB-T2, showing that the proposed algorithm has reduced complexity with respect to TR, ACE, and CF, mainly because our solution is one-shot and does not require iterations.

The remainder of this paper is organized as follows. Section II briefly introduces the system model, while Section III describes the proposed algorithm in detail. In Section IV, we compare the computational complexity of the proposed method with conventional TR, ACE, and CF methods. The theoretical performance of the additional data stream inserted in the reserved carriers for purposes of PAPR reduction is presented in Section V. Section VI discusses the simulated PAPR performance and the computational complexity, and compares the proposed method with conventional TR, ACE, and CF methods. Section VII concludes the paper.

II. SYSTEM MODEL

Fig. 1 shows the considered DVB-T2 system model. After channel coding (a concatenation of BCH and LDPC codes [4]), data are multiplexed, together with pilot data and reserved carriers, in the time-frequency domain. Each OFDM symbol contains $N_a = N_d + N_p + N_s$ active carriers, where N_d carriers transport the data, N_p carriers are pilot carriers, and N_s reserved carriers are available for the insertion of a correction signal to reduce the signal peaks: we will use these reserved carriers also to convey additional signaling bits.

We now introduce the mathematical model of the DVB-T2 data signal, omitting for simplicity the P1, P2, and FEF parts. The l -th discrete-time baseband OFDM symbol can be expressed as

$$x[n, l] = \frac{1}{\sqrt{LN}} \sum_{k=0}^{N_a-1} X[k, l] e^{j \frac{2\pi}{LN} (k+K_0)n} \quad (1)$$

for $n \in \{-LN_\Delta, \dots, LN - 1\}$ and 0 elsewhere, with $l \in \{0, \dots, N_F - 1\}$ the time index of the OFDM symbol, N_F the number of OFDM symbols in a data frame, L the oversampling factor, N the total number of carriers in the OFDM symbol, N_Δ the size of the cyclic prefix before oversampling, $k \in \{0, \dots, N_a - 1\}$ the frequency index, $X[k, l]$ the frequency-domain signal, and K_0 the signal spectrum offset. Thus, the oversampled digital DVB-T2

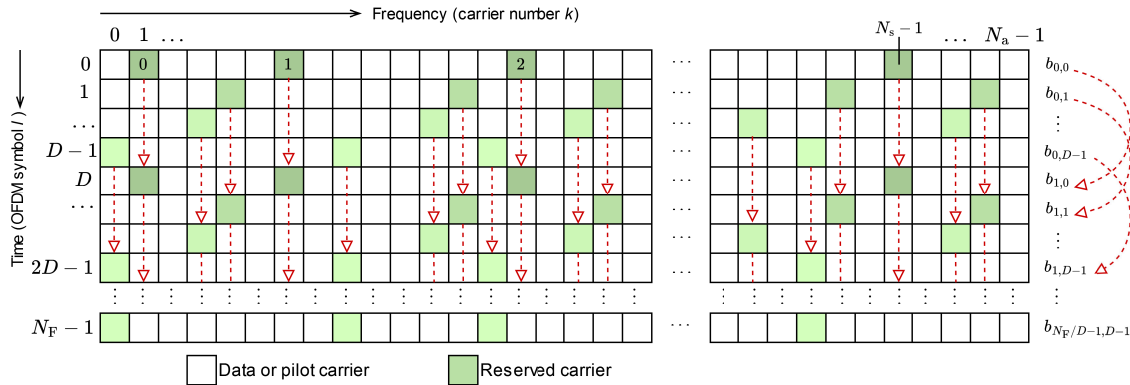


FIGURE 2. Conceptual layout of the proposed TR scheme: the green hues denote the d -th binary sequence, and the dashed arrows indicate the direction of differential PSK encoding.

signal is given by concatenating the N_F blocks, as expressed by

$$z[n] = \sum_{l=0}^{N_F-1} x[n-lL(N + N_\Delta), l],$$

where $n \in \{-LN_\Delta, \dots, N_FL(N + N_\Delta) - LN_\Delta - 1\}$ is the discrete time index that spans the whole data part. Using an oversampling factor $L > 1$, the oversampled digital signal better approximates the analog signal, so that the PAPR estimation is more accurate than for $L = 1$. The choice of L is a trade-off between complexity and accuracy; it was shown in [6] that $L = 4$ is a good choice.

Note that the N_s reserved carriers can be exploited to reduce the peaks of $x[n, l]$. Inspired by the signaling of DVB-T [72], [73], we insert in the reserved carriers a differential binary phase-shift keying (DBPSK) signal, modulated among successive OFDM symbols, with repetition factor of N_s in the frequency domain (Fig. 2). Since the positions of the DVB-T2 reserved carriers periodically repeat every D OFDM symbols [4], in a frame with N_F OFDM symbols we use D different bit sequences, each with length N_F/D symbols. We denote with $b_{q,d}$ the q -th bit of the d -th binary sequence ($b_{0,d} = 0$ is the reference bit of the d -th sequence). The additional DBPSK-modulated data signal can be expressed as

$$X_s[i, l] = 1 - 2 a_{i,l}, \quad (2)$$

$$a_{i,l} = r_{K_s[i,l]} \oplus c_l, \quad (3)$$

$$c_{Dq+d} = c_{D(q-1)+d} \oplus b_{q,d}, \quad (4)$$

where $i \in \{0, \dots, N_s - 1\}$ is the index for the reserved carriers, $l \in \{0, \dots, N_F - 1\}$ is the time index of the OFDM symbol, $q \in \{0, \dots, N_F/D - 1\}$ is the time index of each additional bit sequence, $d \in \{0, \dots, D - 1\}$ is the sequence number, c_l is the l -th differentially encoded bit repeated on the N_s carriers, $a_{i,l}$ is the scrambled bit on the i -th reserved carrier of the l -th OFDM symbol, r_k is the frequency-domain scrambling (energy dispersal) sequence [4], $k \in \{0, \dots, N_a - 1\}$, \oplus is the exclusive or (xor) operator, and $\{K_s[i, l]\}_{i=0}^{N_s-1}$ is the set of indexes of the reserved carriers. This set of reserved carrier indexes is a subset of the active carrier

indexes $\{0, \dots, N_a - 1\}$, with preassigned indexes that change with the OFDM symbol index l and periodically repeat every D OFDM symbols [4], i.e., $K_s[i, l] = K_s[i, l + D]$. Note that (2) represents the mapping operation, (3) is the frequency-domain repetition coding with scrambling, and (4) stands for the differential encoding. The reserved carriers (2) are multiplexed into the frequency domain signal $X[k, l]$ used in (1) by means of the indexing function $k = K_s[i, l]$, as expressed by

$$X[K_s[i, l], l] = X_s[i, l], \quad i = 0, \dots, N_s - 1. \quad (5)$$

III. PAPR REDUCTION ALGORITHM

This section explains how the data signal (2)–(4), inserted on the DVB-T2 reserved carriers (5), is modified by the proposed algorithm to reduce the PAPR of the generated DVB-T2 signal (1).

The idea of the proposed algorithm is to conveniently select a subset \mathcal{K}_H of the index set $\{K_s[i, l]\}_{i=0}^{N_s-1}$ of reserved carriers, whose amplitude will be amplified, and to simultaneously clip to zero the amplitudes on the complementary set $\bar{\mathcal{K}}_H$ of reserved carriers. Our method will select the subset \mathcal{K}_H and the associated amplitude weight in such a way to reduce the PAPR. The proposed method does not destroy the information contained in $X_s[i, l]$, because the binary phase is left unchanged on the carriers belonging to \mathcal{K}_H , while repetition coding will help to recover the DBPSK data despite the carriers belonging to $\bar{\mathcal{K}}_H$ will be zeroed. Mathematically, the proposed algorithm replaces (5) with

$$X[K_s[i, l], l] = W[l]\mathcal{H}[i, l]X_s[i, l], \quad i = 0, \dots, N_s - 1, \quad (6)$$

where $\mathcal{H}[i, l]$ is a carrier selection function that can be 0 or 1 and $W[l]$ is an amplitude weight common to all the selected carriers. From now on, to simplify the notation, we omit the OFDM symbol index l whenever possible.

A. WORKING PRINCIPLE OF THE PROPOSED ALGORITHM

The working principle of the proposed algorithm is explained below. For a given information signal associated to the data carriers, the additional DBPSK data transmitted on the

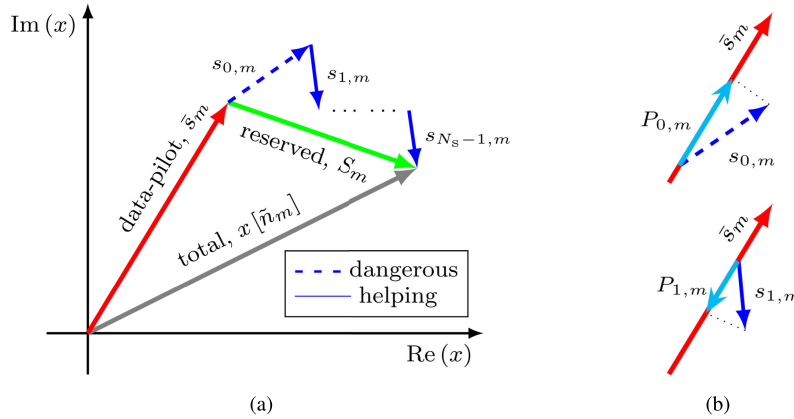


FIGURE 3. (a) Composition of the time-domain peak $x[\tilde{n}_m]$ as the sum of two contributions: data-pilot carriers and reserved carriers; (b) projections of additional data contributions onto the data-pilot contribution: dangerous contribution at the top, helping contribution at the bottom.

reserved carriers may contribute or prevent possible peaks in the time domain, depending on whether each reserved carrier adds constructively (in-phase) or destructively (counter-phase) with the overall information signal. Thus, the proposed algorithm nullifies those reserved carriers whose signal adds constructively to the data carriers in those time indexes that correspond to the M highest peaks. At the same time, the proposed algorithm maintains the additional data on the reserved carriers whose signal adds destructively on the data carriers: this reduces the M highest peaks. Despite the DBPSK signal has been nulled on some reserved carriers, the additional data can still be recovered thanks to repetition coding, because the power scaling on the other reserved carriers does not alter the phase of the DBPSK signal.

Mathematically, the proposed algorithm can be explained as follows. We start by defining the ratio between the m -th largest peak power and the average power, denoted as m -PAPR, expressed by

$$\rho_m = \frac{\max_m \{y[n]\}}{\mu_y}, \quad (7)$$

where $y[n] = |x[n]|^2$, $n \in \{0, \dots, LN - 1\}$, is the instantaneous power of the OFDM signal (1), $\max_m \{\cdot\}$ is the m -th largest element operator and $\mu_y = E\{y[n]\} = E\{|x[n]|^2\}$, where $E\{\cdot\}$ denotes the expected value. Note that the 1-PAPR $\rho_1 = \rho$ is the classic definition of PAPR, while the 2-PAPR ρ_2 would be the PAPR obtained after reducing the first peak below the second peak. Our method aims at reducing not only $\rho = \rho_1$, but also the m -PAPR ρ_m with $m > 1$, by reducing the largest peaks of the time-domain signal (1).

To keep the PAPR ρ below a given value $\hat{\rho}$, the algorithm must attenuate the peaks with power above the threshold $T = \hat{\rho}\mu_y$. To this purpose, we define the set

$$\mathcal{P}_M = \{\tilde{n}_m, m = 1, \dots, M \mid y[\tilde{n}_m] > T\} \quad (8)$$

of M indexes of those peaks with instantaneous power exceeding T . Note that the set in (8) relates the number M of largest peaks to the PAPR threshold $\hat{\rho} = T/\mu_y$.

Consequently, our algorithm uses the parameter M instead of T . The peak value $x[\tilde{n}_m]$ in (1) is the sum of two contributions: the first, \bar{s}_m , caused by the data-plus-pilot signal, will be kept fixed, while the second, s_m , caused by the additional data on the reserved carriers, will be adjusted to reduce the PAPR. Fig. 3a displays $x[\tilde{n}_m] = \bar{s}_m + s_m$. The contribution of the i -th additional data $X_s[i]$ to the m -th peak $x[\tilde{n}_m]$ in (1) is

$$s_{i,m} = \frac{1}{\sqrt{LN}} X_s[i] e^{j\frac{2\pi}{LN}(K_s[i] + K_0)\tilde{n}_m}, \quad (9)$$

where $K_s[i]$ is the frequency index of the i -th additional bit. Therefore, $s_m = \sum_{i=0}^{N_s-1} s_{i,m}$ is the total contribution of all the additional signaling carriers to the m -th peak, while

$$\bar{s}_m = x[\tilde{n}_m] - s_m = x[\tilde{n}_m] - \sum_{i=0}^{N_s-1} s_{i,m} \quad (10)$$

is the contribution of the data and pilot carriers (Fig. 3a).

Let us denote N_h as the number of reserved carriers in the set \mathcal{K}_H ; therefore, the size of the complementary set $\bar{\mathcal{K}}_H$ is $N_s - N_h$. Let $\mathcal{H}[i] \in \{0, 1\}$ be a carrier selection function, which will be determined in Section III-C, such that $N_h = \sum_{i=0}^{N_s-1} \mathcal{H}[i]$. We denote W a common positive weight that multiplies the signal component of the N_h reserved carriers selected to compensate the PAPR, while the remaining $N_s - N_h$ reserved carriers are nulled. Hence, the time-domain signal $x[\tilde{n}_m] = \bar{s}_m + s_m$ is transformed into $x[\tilde{n}_m] = \bar{s}_m + Wh_m(\mathcal{H})$ where $Wh_m(\mathcal{H}) = W \sum_{i=0}^{N_s-1} \mathcal{H}[i]s_{i,m}$ is the contribution of the reserved carriers after subset selection and amplitude weighting. Therefore, $\max\{|\bar{s}_m + Wh_m(\mathcal{H})|^2\}_{m=1}^M$ represents the numerator of the PAPR in (7) after selection and weighting. Consequently, the PAPR metric becomes

$$J(W, \mathcal{H}) = \max\{|\bar{s}_m + Wh_m(\mathcal{H})|^2\}_{m=1}^M. \quad (11)$$

When the number of carriers N is large, the cancellation of few peaks does not alter significantly the average power μ_y of the OFDM signal, i.e., the denominator of the PAPR in (7): this is also confirmed by the simulation results in Section VI (see Tab. 1). Hence, a PAPR reduction strategy aiming at

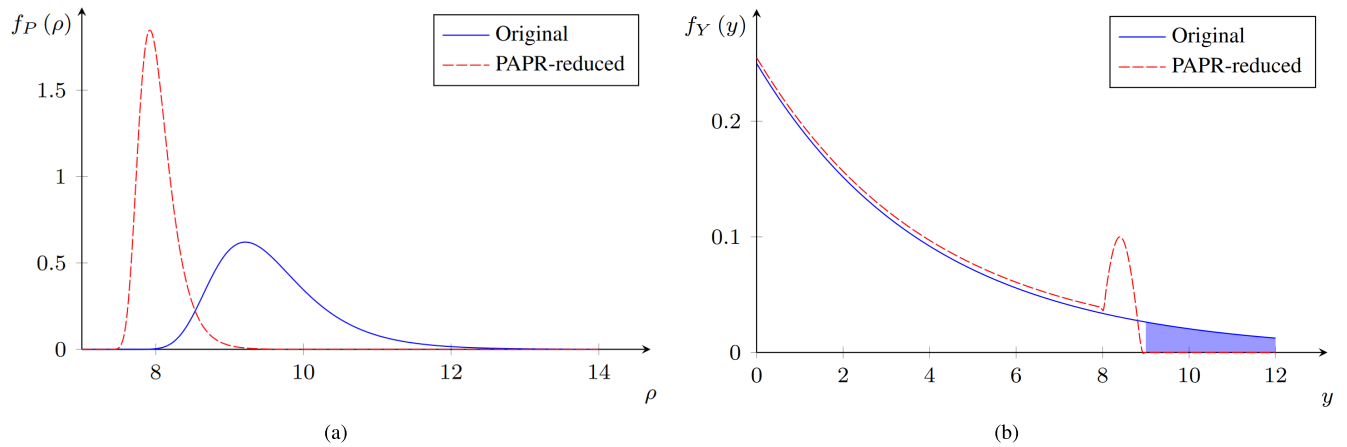


FIGURE 4. (a) Sketch of a possible pdf of the PAPR ρ ; (b) sketch of a possible pdf of the instantaneous power y .

reducing the m -PAPR (with $1 \leq m \leq M$) in (7) should minimize J in (11).

The minimization of (11) gives the *optimal power weighting* (OPW) W_O and the *optimal selection function* (OSF) \mathcal{H}_O for m -PAPR reduction. We follow a three-step approach: first, we simplify the PAPR metric J of (11) with \hat{J} , which corresponds to the sum of the m -PAPR metrics in (7); second, we find the OSF $\hat{\mathcal{H}}_O$ using the simplified metric \hat{J} ; and finally we find the OPW \hat{W}_O for the original metric J using the obtained OSF $\hat{\mathcal{H}}_O$. The obtained function $\hat{\mathcal{H}}_O$ and the obtained weight \hat{W}_O are then used in (6) to produce a PAPR-reduced signal (1).

B. FIRST STEP: METRIC SIMPLIFICATION

Our aim is to reduce the m -PAPR ρ_m in (7), for $m = 1, \dots, M_P$, with $1 \leq M_P \leq M$. M_P is a design parameter that denotes the size of the largest peaks in \mathcal{P}_M : its value can be determined, for instance, by selecting those peaks that exceed a given threshold T_P , with $T_P > T$. The reason for the introduction of another design parameter M_P , with $M_P \leq M$, can be explained as follows. While the largest peaks determine the PAPR, the reduction of the largest peaks may produce a regrowth of other peaks. Here we want to reduce the largest M_P peaks and concurrently we want to avoid the regrowth of the other $M - M_P$ peaks. Hence we need two parameters: the largest M_P peaks will be used in Section III-C for reserved carrier selection aiming at reducing the largest peaks, while the extended set of M peaks will be used in Section III-D for optimal weighting aiming at avoiding the regrowth of other peaks.

Note that $\max\{y[\tilde{n}_m]\}_{m=1}^M = \max\{y[\tilde{n}_m]\}_{m=1}^{M_P}$, since the M_P peaks are the largest among the M peaks. In order to simplify the metric in (11), we use the inequality

$$\max\{y[\tilde{n}_m]\}_{m=1}^{M_P} \leq \sum_{m=1}^{M_P} y[\tilde{n}_m] \leq M_P \max\{y[\tilde{n}_m]\}_{m=1}^{M_P}.$$

In the above equation, the minimization of the first term or the third term is equivalent, therefore also the second term

can be used as a cost function to minimize the PAPR. Thus, we replace the maximum in (11) with the sum, to obtain the approximation

$$\begin{aligned} \hat{J}(W, \mathcal{H}) &= \sum_{m=1}^{M_P} |\bar{s}_m + Wh_m(\mathcal{H})|^2 \\ &= \sum_{m=1}^{M_P} y[\tilde{n}_m] = \mu_y \sum_{m=1}^{M_P} \rho_m, \end{aligned} \tag{12}$$

which is proportional to the sum of the first M_P m -PAPR's in (7). Differently from J in (11), \hat{J} in (12) uses a sum to replace the maximum: therefore, the minimization of \hat{J} is easier than that of J , because the differentiation of \hat{J} admits a closed-form solution.

The approximated metric (12) is explained in the following. Under the hypotheses of stationarity and ergodicity of $y[n] = |x[n]|^2$, the sum in (12) is, in the limit for $M_P \rightarrow \infty$,

$$\lim_{M_P \rightarrow \infty} \frac{1}{M_P} \sum_{m=1}^{M_P} y[\tilde{n}_m] = E\{y[n] \mid y[n] > T_P\} \propto \int_{T_P}^{+\infty} y f_Y(y) dy \tag{13}$$

where \tilde{n}_m is the index for the M_P peaks that exceed the threshold T_P , $f_Y(y)$ is the pdf of the instantaneous power, and \propto means *proportional to*. Fig. 4 shows the pdf $f_P(\rho)$ of the PAPR calculated as in [74] and the pdf $f_Y(y)$ of the instantaneous power. Every PAPR reduction scheme shifts part of the PAPR pdf $f_P(\rho)$ to the left, as shown by the dashed red curve in Fig. 4a. This is equivalent to the cancellation of the shaded area in the pdf $f_Y(y)$ of the instantaneous power in Fig. 4b. This shaded area is expressed by

$$\text{Prob}\{y[n] > T_P\} = \int_{T_P}^{+\infty} f_Y(y) dy, \tag{14}$$

while the approximated metric $\hat{J}(W, \mathcal{H})$ in (12)–(13) includes a weight y into the integral. With reference to Fig. 4b, a PAPR reduction scheme annihilates the integral in (14), or the integral in (13) that uses a larger weight for a bigger peak.

Instead of (14), the proposed algorithm minimizes the sum of m -PAPR's in (13), because bigger peaks require more reduction than the other peaks.

C. SECOND STEP: OPTIMAL SELECTION OF THE RESERVED CARRIERS

By differentiating (12) with respect to W and setting to zero, we find the weight

$$W^+(\mathcal{H}) = \frac{-\sum_{m=1}^{M_p} p_m(\mathcal{H})}{\sum_{m=1}^{M_p} |h_m(\mathcal{H})|^2} = \frac{-\sum_{i=0}^{N_s-1} \mathcal{H}[i] \sum_{m=1}^{M_p} p_{i,m}}{\sum_{m=1}^{M_p} |h_m(\mathcal{H})|^2}, \quad (15)$$

with $h_m(\mathcal{H}) = \sum_{i=0}^{N_s-1} \mathcal{H}[i] s_{i,m}$, $p_m(\mathcal{H}) = \sum_{i=0}^{N_s-1} \mathcal{H}[i] p_{i,m}$, and

$$p_{i,m} = \text{Re}(\bar{s}_m) \text{Re}(s_{i,m}) + \text{Im}(\bar{s}_m) \text{Im}(s_{i,m}). \quad (16)$$

In (15), $h_m(\mathcal{H})$ is the additional data contribution and in (16) $p_{i,m}$ is the projection of the contribution $s_{i,m}$ in (9) onto the data-pilot contribution \bar{s}_m , as shown in Fig. 3b. Note also that, by substituting back (15) in (12), we resort to an integer optimization problem.

The carrier selection function $\mathcal{H}[i]$, used in (15), is determined as follows. Since $W > 0$, to avoid negative values of $W^+(\mathcal{H})$ in (15), $\mathcal{H}[i]$ selects the reserved carriers with negative sum projection $\sum_{m=1}^{M_p} p_{i,m}$ in (15); hence, the OSF is

$$\hat{\mathcal{H}}_O[i] = \begin{cases} 1, & \text{for } i \in \{0, \dots, N_s - 1\} \mid \sum_{m=1}^{M_p} p_{i,m} < 0, \\ 0, & \text{elsewhere.} \end{cases} \quad (17)$$

As shown in Fig. 3b, the N_h reserved carriers with negative sum projection $\sum_{m=1}^{M_p} p_{i,m}$ contribute to a peak reduction and hence are *helping*; differently, the $N_s - N_h$ reserved carriers with positive projection produce a peak increase and therefore are *dangerous*. Using the OSF in (17), the positive weight $W^+(\hat{\mathcal{H}}_O)$ amplifies the helping carriers, which reduce the PAPR, and the selection function $\hat{\mathcal{H}}_O[i]$ nulls the dangerous carriers, in order to avoid the PAPR regrowth.

D. THIRD STEP: OPTIMAL WEIGHT

With a chosen OSF $\hat{\mathcal{H}}_O[i]$, we can now minimize (11) with respect to W : as detailed in Appendix A, the global minimum of $J(W, \hat{\mathcal{H}}_O)$ occurs either in one of the M minima of each parabola $|\bar{s}_m + W h_m(\hat{\mathcal{H}}_O)|^2$, or in one of the $M^2 - M$ intersections between all pairs of parabolas, as expressed, respectively, by

$$W_{\min}^{(m)} = -\frac{B_m}{2A_m}, \quad W_{\mp}^{(m,n)} = \frac{-(B_m - B_n) \mp \sqrt{\Delta^{(m,n)}}}{2(A_m - A_n)}, \quad (18)$$

$$\Delta^{(m,n)} = (B_m - B_n)^2 - 4(A_m - A_n)(C_m - C_n), \quad (19)$$

with $A_m = |h_m(\hat{\mathcal{H}}_O)|^2$, $B_m = 2\text{Re}[\bar{s}_m h_m^*(\hat{\mathcal{H}}_O)]$, $C_m = |\bar{s}_m|^2$, and $m \neq n$. In Appendix A we also present a search algorithm that reduces the number of intersections and minima to be

Algorithm 1 OSF-OPW PAPR Reduction Algorithm

- 1: **for all** l (OFDM symbol index) **do**
- 2: DBPSK: $X_s[i, l]$ using (2)–(4)
- 3: $x[n, l] \leftarrow \text{IFFT}(X[k, l])$ using (1) with (5)
- 4: M peak indexes: $\tilde{n}_m \leftarrow \arg \max_m \{|x[n, l]|\}$
- 5: MN_s contributions: $s_{i,m}$ using (9)
- 6: M total contributions: \bar{s}_m using (10)
- 7: $M_p N_s$ projections: $p_{i,m}$ using (16)
- 8: OSF: $\hat{\mathcal{H}}_O[i]$ using (17)
- 9: OPW: \hat{W}_O using (20) with (18)–(19) and Appendix A
- 10: $x[n, l] \leftarrow \text{IFFT}(X[k, l])$ using (1) with (6)
- 11: **end for**

explored from M^2 to $M_{\text{eff}}M$, with $M_{\text{eff}} \ll M$. The final optimal weight for OPW becomes

$$\hat{W}_O = \arg \min_{W \in W_{\min}^{(m)} \cup W_{\mp}^{(m,n)}} J(W, \hat{\mathcal{H}}_O). \quad (20)$$

The use of the weight \hat{W}_O in (20) increases the power of $x[n]$ in (1): simulations in a typical scenario show a 2.6% or 0.1 dB power increase, as detailed in Section VI. The power increase is small because the weight is applied to the reserved carriers only. In any case, the power increase can be controlled in two ways. A first strategy consists in limiting the maximum permitted value of \hat{W}_O : this can be done by excluding from (20) those weights in (18) that exceed a predetermined threshold W_{th} that controls the maximum allowable power increase. A second strategy simply avoids the OPW (20) and selects the weight according to a predetermined power increase: for instance, if we desire to not increase the power, we can adopt a *same power weighting* (SPW) strategy, which replaces \hat{W}_O with $W_s = \sqrt{N_s/N_h}$.

E. SUMMARY OF THE PROPOSED ALGORITHM

The proposed OSF-OPW algorithm, detailed in Sections III-B, III-C, and III-D, is summarized in Algorithm 1. Since QAM data and pilot carriers are left unchanged by the algorithm, the proposed PAPR reduction algorithm will not degrade the modulation error ratio (MER) on the data carriers. Note that the proposed algorithm does not require side information at the receiver, because the receiver will perform the recovery of the DBPSK additional data without knowledge of which reserved carriers are amplified or zeroed.

IV. COMPUTATIONAL COMPLEXITY

Computational complexity has a significant effect on the power consumption of the digital section of the modulator. Herein we evaluate the computational complexity of the proposed PAPR reduction algorithm and of some alternative techniques. In this computation, we omit the complexity of all the transmitting blocks that are common to all the PAPR reduction techniques (channel coding, interleaving, QAM mapping, multiplexing, IFFT of OFDM, cyclic prefix insertion, etc.). The complexity is calculated as the number

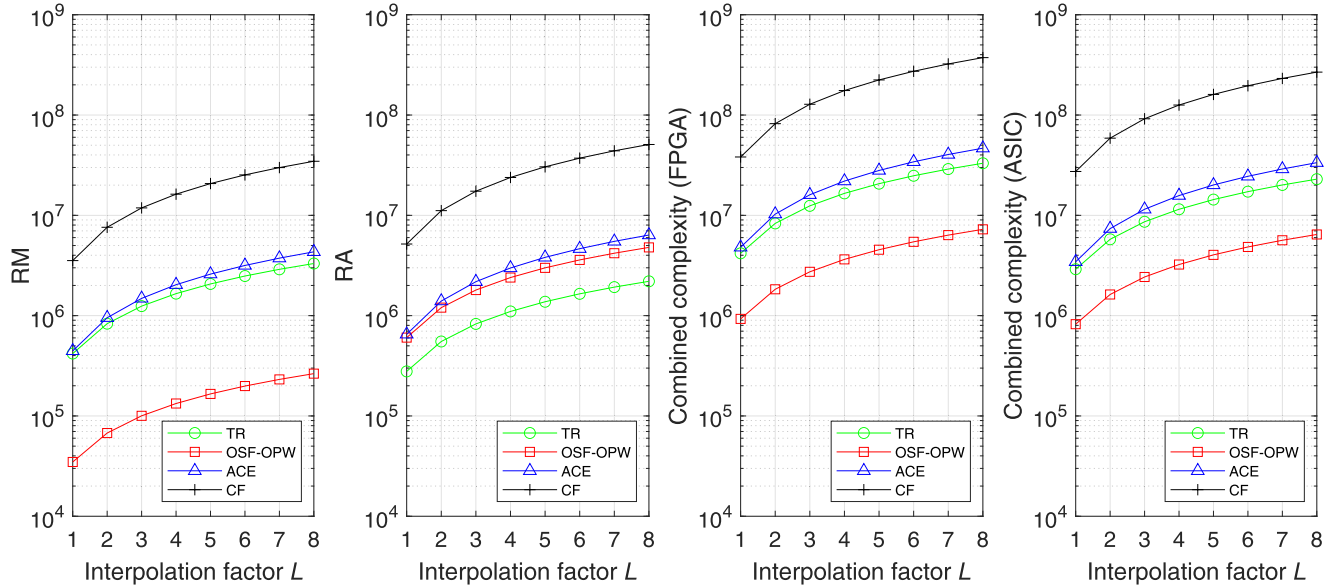


FIGURE 5. Computational complexity of the compared PAPR reduction techniques.

of real multiplications (RM), real additions (RA), and value comparisons (VC) of each algorithm. The cost of a complex multiplication is obviously equal to 4 RM plus 2 RA, whereas we count a square root operation or a real division as 1 RM. We also assume that the twiddle factors $E_{LN}^k = e^{j2\pi k/(LN)}/\sqrt{LN}$ for OSF-OPW and the kernels for the TR method are precomputed, and that sign inversions, multiplications by powers of two, and sign comparisons have negligible cost. In the following, we provide the total estimated cost for each compared technique (details are reported in Appendix B).

A. COMPUTATIONAL COST OF OSF-OPW

We neglect the cost of the simple binary and mapping operations for DBPSK in (2)–(4). To reduce the computational complexity, instead of using (1) with (6), the OSF-OPW algorithm is equivalently implemented by first constructing the original signal (1) with (5) and by successive addition of a correction signal, expressed by

$$x_C[n, l] = \hat{W}_O[l] \sum_{i=0}^{N_s-1} \hat{H}_O[i, l] X_s[i, l] E_{LN}^{(K_s[i, l]+K_O)(n-ILN_\Delta)} - \sum_{i=0}^{N_s-1} X_s[i, l] E_{LN}^{(K_s[i, l]+K_O)(n-ILN_\Delta)}, \quad (21)$$

that produces the same result of (6).

By combining DBPSK modulation, scrambling, and reserved carrier selection, and using an oversampling factor $L = L_{OSF}$, the proposed OSF-OPW method requires $4L_{OSF}N + 2N_sM_P + M_{eff}(3M + 4) + 8M$ RM, $L_{OSF}N(N_s + 1) + N_s(2(M + M_P) - 1) + 7M + 4M_{eff}M$ RA, and $M(L_{OSF}N - 1) + M_{eff}(2M + 3) - 1$ VC. For $M < N_s$, the complexity order for RM of OSF-OPW is $\mathcal{O}(L_{OSF}N + M_P N_s)$, and it is mainly due to the identification of the peaks to be canceled

and to the generation of the correction signal, as detailed in Appendix B.

B. COMPUTATIONAL COST OF ALTERNATIVE TECHNIQUES

The cost of the TR method described in the DVB-T2 standard [4] depends on the average number of iterations M_{TR} required to cancel out the peaks exceeding a clipping value $V_{CLIP,TR}$. Using an oversampling factor $L = L_{TR}$, the total cost is $M_{TR}(8L_{TR}N + 13N_s + 2)$ RM, $2L_{TR}N + M_{TR}(5L_{TR}N + 8N_s + 3)$ RA, and $M_{TR}(L_{TR}N + N_s)$ VC, with a complexity order for RM of $\mathcal{O}(M_{TR}L_{TR}N)$. Details are given in Appendix B.

The complexity of the ACE method described in Clause 9.6.1 of [4, p. 117] depends on the average number of peaks M_{ACE} that exceed a clipping value $V_{CLIP,ACE}$ and on the average number of extendable constellation points, which is $N_{d,ext} \approx N_d(2\sqrt{M_{qam}} - 3)/M_{qam}$. Globally, assuming an oversampling factor $L = L_{ACE}$, the ACE technique requires $4L_{ACE}N \log_2(L_{ACE}N) + 2L_{ACE}N + 2N_{d,ext} + 4M_{ACE}$ RM, $6L_{ACE}N \log_2(L_{ACE}N) + L_{ACE}N + 4N_{d,ext}$ RA, and $L_{ACE}N + 10N_{d,ext}$ VC, with a complexity order for RM of $\mathcal{O}(L_{ACE}N \log_2(L_{ACE}N))$. Details are in Appendix B.

In addition to the techniques described in the DVB-T2 standard, we also consider the CF algorithm of [8]. Assuming an oversampling factor $L = L_{CF}$ and a number of iterations M_{CF} , the CF technique requires about $4M_{CF}L_{CF}N \log_2(L_{CF}N) + 2M_{CF}L_{CF}N$ RM, $6M_{CF}L_{CF}N \log_2(L_{CF}N) + M_{CF}L_{CF}N$ RA, and $M_{CF}L_{CF}N$ VC, with a complexity order of $\mathcal{O}(M_{CF}L_{CF}N \log_2(L_{CF}N))$ for RM. Most of the complexity is due to the FFT and IFFT operations, which require $4L_{CF}N \log_2(L_{CF}N)$ RM and $6L_{CF}N \log_2(L_{CF}N)$ RA per iteration.

C. COMPARISON OF COMPUTATIONAL COSTS

Fig. 5 compares the four techniques under investigation (OSF-OPW, TR, ACE, and CF) in terms of RM and

RA complexity as a function of the interpolation factor. In addition, Fig. 5 also shows the combined complexity, evaluated as a weighted average of RA and RM. According to [75], the weights for RA and RM are 1.0 and 9.3264, respectively, for FPGA-based implementation, and 1.0 and 6.2711, respectively, for ASIC-based implementation [75]. In Fig. 5, we used a typical DVB-T2 setting with $M_P = 10$, $M = 27$, and $M_{\text{eff}} \approx 4$ (the values of the other parameters are detailed in Section IV), but the results of the comparison would be similar also for other settings. From Fig. 5, it is clear that OSF-OPW has a computational advantage over the other techniques, in terms of RM and combined complexity. Although the number of RA of the proposed algorithm is somewhat larger than for TR, our method is less complex because an RM is significantly more costly than an RA [75], [76, p. 320]. As a consequence of the reduced complexity, the latency of the proposed method is not larger than that of the other compared methods.

V. THEORETICAL BER OF THE ADDITIONAL DATA

This section focuses on the BER performance of the additional data inserted in the reserved carriers. The additional data bits on the reserved carriers are DBPSK modulated along the time direction and repeated over N_s reserved carriers. We focus on additive white Gaussian noise (AWGN) channels. If all the reserved carriers are used with the same power, the theoretical bit error rate (BER) of the additional bits is expressed as in [77, p. 740, eqs. (11.1-13)–(11.1-14)], using N_s independent channels. When some reserved carriers are nulled, the theoretical BER can be derived by generalizing (to non-identically distributed variables) the results described in Appendix B of [77, p. 1090–1095]. In this case, for $N_h = N_s/2$ and a random assignment of the helping carriers, the generalization of [77, p. 1094, eq. (B-21)] produces the theoretical BER

$$P_b = Q_1 \left(\sqrt{\frac{1}{4} N_s \gamma}, \sqrt{\frac{3}{4} N_s \gamma} \right) - \frac{1}{2} e^{-\frac{N_s \gamma}{2}} I_0 \left(\frac{\sqrt{3}}{4} N_s \gamma \right) + \frac{e^{-\frac{N_s \gamma}{2}}}{4^{N_s-1}} \sum_{n=1}^{N_s-1} \sinh \left(\frac{n \log_e 3}{2} \right) I_n \left(\frac{\sqrt{3}}{4} N_s \gamma \right) \sum_{k=0}^{N_s-1-n} \binom{2N_s-1}{k}, \quad (22)$$

where $Q_1(\cdot, \cdot)$ is the Marcum Q function of first order, $I_n(\cdot)$ is the modified Bessel function of the first kind and order n , $\gamma = \Gamma/F$ is the SNR on the reserved carriers, Γ is the overall carrier-to-noise ratio (CNR) of the DVB-T2 signal (including the power of data, pilots, and reserved carriers), and F is a correction factor to include the power of the N_p pilot carriers. The derivation of (22) is detailed in Appendix C.

VI. SIMULATION RESULTS

We choose the following DVB-T2 parameters [4]: frame with length $N_F = 68$ OFDM symbols; 8K mode with FFT size $N = 8192$, number of active carriers $N_a = 6817$, number of reserved carriers $N_s = 72$ (for ACE, $N_s = 0$), and cyclical repetition period of the reserved carriers

$D = 4$; 64-QAM, i.e., constellation size $M_{\text{qam}} = 64$; DVB-T2 forward error correction with code rate $R_c = 3/4$ and PP5 pilot pattern, which gives $N_d = 6562$ data carriers (for ACE, $N_d = 6634$) and $N_p = 183$ pilot carriers [4]. These parameters produce a pilot power correction factor $F = (N_d + 5.8634 N_p + N_s)/N_a = 1.1306$. For low-complexity OSF methods, we select an oversampling factor $L = L_{\text{OSF}} = 4$. For TR and ACE, we select $L = L_{\text{TR}} = 1$ and $L = L_{\text{ACE}} = 4$, respectively: these are the values specified in the DVB-T2 standard [4, pp. 116–121]. For CF, $L = L_{\text{CF}} = 4$. In all cases, the PAPR is measured on the four-times oversampled signal.

A. PAPR COMPARISON

Fig. 6 shows the complementary cumulative distribution function (CCDF) $\bar{F}_P(\rho) = 1 - F_P(\rho)$ of the PAPR for the proposed OSF-OPW method, for different values of the number of cancelled peaks M_P . The parameter M is empirically limited to $M = M_P + 17$: therefore, the proposed algorithm tries to cancel the largest M_P peaks while avoiding the regrowth of the largest $M = M_P + 17$ peaks. Note that M_P is the subset of largest peaks used by the OSF in (12) and in (17), while M is the extended set of peaks used by the OPW in (11) and in (20): indeed, the selection of the reserved carriers is guided by the largest peaks only, while the selection of the weight must ensure that also the other $M - M_P$ peaks do not regrow. To keep complexity under control, we have assumed a fixed value for $M - M_P = 17$ for all the cases. To control the power increase, the OSF-OPW algorithm uses a threshold $W_{\text{th}} = 5$, which produces a 2.6% increase of signal power, as shown in Tab. 1 for a typical simulation scenario. As highlighted by Fig. 6, when the number of canceled peaks raises up to $M_P = 10$, the PAPR reduces; then, when the number of canceled peaks increases further, the PAPR does not reduce anymore and tends to increase. This behavior can be explained as follows. When the number of canceled peaks M_P is small, the increase of M_P improves the correct identification of the helpful reserved carriers. However, since the signs of the projections $p_{i,m}$ may be different for different peaks (i.e., for different m), when the number of canceled peaks M_P increases further, the number of reserved carriers that are helpful for all the M_P peaks reduces, and the selection of the reserved carriers inevitably must include some carriers that are dangerous for some peaks. Indeed, we should bear in mind that the number $N_s = 72$ of reserved carriers is low, compared with the number of active carriers $N_a = 6817$.

Fig. 7 highlights the obtained PAPR ρ' at $\bar{F}_P(\rho) = 10^{-4}$ as a function of M_P . To better appreciate the behavior of the curve in Fig. 7, we have rounded the simulated PAPR results to one tenth of dB. Fig. 7 clearly explains that the optimal value of M_P is around $M_P \approx 8$, and that the nearby values are optimal as well. This behavior helps the selection of the M_P parameter.

Fig. 8 compares the CCDF of the PAPR for different methods. We also include the OSF-SPW method and a random selection function (RSF) OPW method that randomly

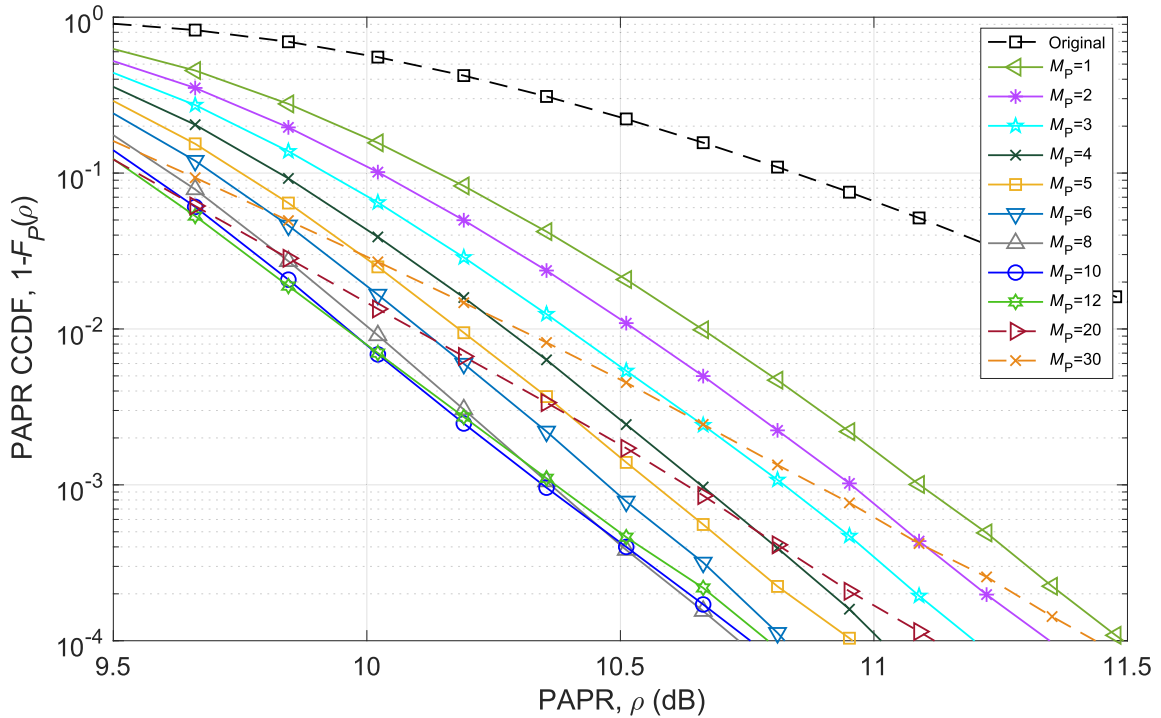


FIGURE 6. CCDF of PAPR for different values of M_p in the OSF-OPW technique ($M = M_p + 17$).

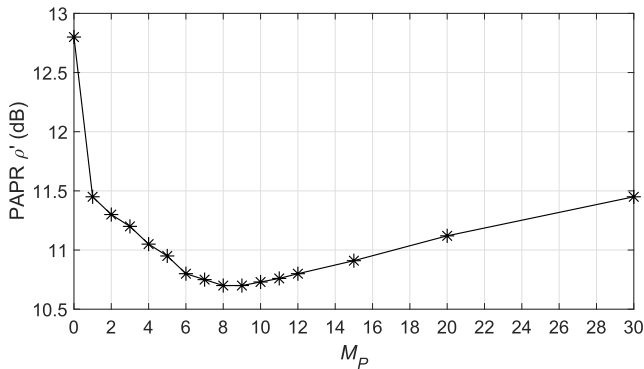


FIGURE 7. OSF-OPW: obtained PAPR ρ' for different values of M_p .

activates $N_h = N_s/2$ reserved carriers. The PAPR ρ' is compared at $\bar{F}_P(\rho') = 10^{-4}$. With respect to the original signal, the PAPR reduction of the proposed OSF-OPW algorithm is 2.1 dB, when $M_p = 10$ and $M = 27$. As shown in Fig. 7, the attempt to cancel more than $M_p = 10$ peaks does not reduce the PAPR further. Fig. 8 also shows that the OSF-SPW method is suboptimal, yielding a PAPR reduction of 1.0 dB only (with respect to the original signal): therefore, the proposed OPW approach outperforms the SPW approach, thereby confirming the correctness of our proposed weighting strategy. In addition, Fig. 8 reveals that the RSF-OPW approach gives a bad result with almost no PAPR reduction: this confirms the correctness of our proposed subset selection strategy.

Fig. 8 also compares the PAPR CCDF for the TR and ACE methods described in the DVB-T2 standard [4, pp. 116–121]. We have exhaustively simulated both TR and ACE techniques

over a wide range of parameters with a fine grid. For both TR and ACE, herein we present the results for the parameters that produce the best PAPR reduction: for TR, $V_{CLIP,TR} = 2.9$ and number of maximum iterations $I_{MAX} = 20$; for ACE, $V_{CLIP,ACE} = 2.2$, gain $G_{ACE} = 10$ and extension limit $L_E = 1.4$ [4]. Since the ACE method can modify up to $N_d = 6562$ carriers, ACE achieves a better PAPR reduction than OSF-OPW, which can modify $N_s = 72$ carriers only. However, ACE is significantly more complex than OSF-OPW. The TR technique of DVB-T2 [4] is less effective than OSF-OPW from the PAPR reduction viewpoint and is also more complex than OSF-OPW. Fig. 8 also includes the PAPR of CF with parameters $M_{CF} = 8$ iterations and $V_{CLIP,CF} = 3.1, 3.4, \text{ and } 3.7$, which produce a MER of 48.8, 57.4, and 66.4 dB, respectively. For $V_{CLIP,CF} = 3.4$, the PAPR ρ' for CF is similar to the PAPR for the proposed OSF-OPW, but the CF introduces a MER of 57.4 dB and has an increased complexity, as detailed in the next sections. The CF algorithm can achieve the PAPR performance of the ACE algorithm by using $V_{CLIP,CF} = 3.1$, at the price of a MER of 48.8 dB and increased data distortion. Differently, the proposed OSF-OPW method does not alter the data. Table 1 compares the PAPR ρ' , the transmitted power μ_y modified by the effect of reserved carriers or extended constellations, and the consequent SNR loss $\Delta_{SNR_{dB}} = 10 \log_{10} \mu_y$ experienced by the QAM data when all the techniques transmit with the same power.

B. COMPLEXITY COMPARISON

Table 1 summarizes the computational costs of the algorithms for the parameters used in Fig. 8. For complexity comparison,

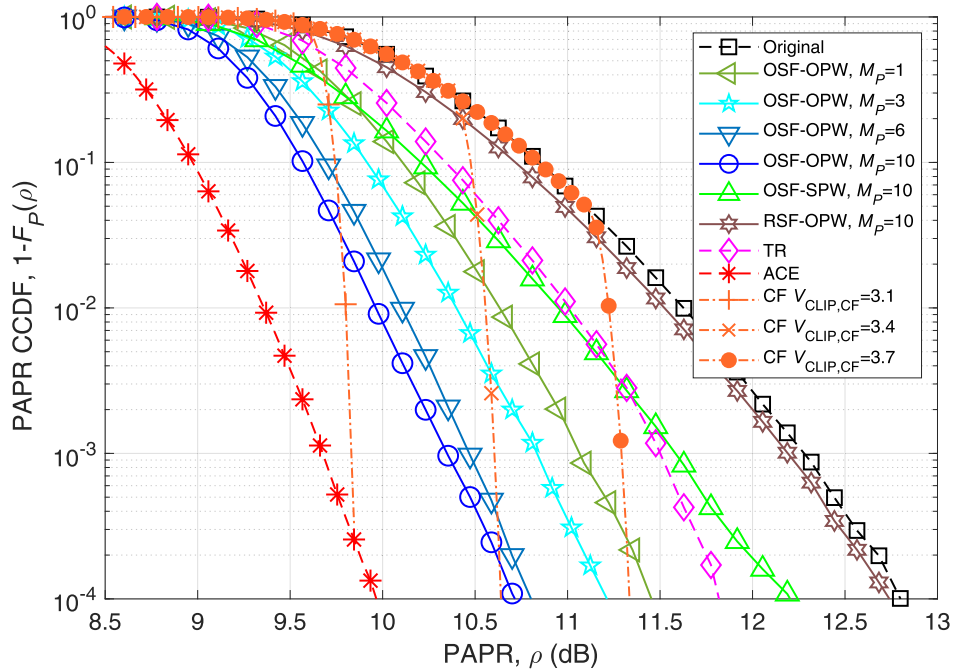


FIGURE 8. Simulated CCDF of the tested DVB-T2 PAPR reduction methods.

TABLE 1. Performance-complexity comparison.

	PAPR ρ'	Signal power μ_y (SNR loss $\Delta_{\text{SNR}_{dB}}$)	RM of PAPR reduction	Complexity order
Original	12.8 dB	100.0% (0.00 dB)	0	–
TR	11.8 dB	100.2% (0.01 dB)	$4.2 \cdot 10^5$	$\mathcal{O}(M_{\text{TR}}L_{\text{TR}}N)$
OSF-OPW	10.7 dB	102.6% (0.11 dB)	$1.3 \cdot 10^5$	$\mathcal{O}(L_{\text{OSF}}N + M_{\text{P}}N_s)$
ACE	10.0 dB	104.8% (0.20 dB)	$2.0 \cdot 10^6$	$\mathcal{O}(L_{\text{ACE}}N \log_2(L_{\text{ACE}}N))$
CF	9.9 dB	100.0% (0.00 dB)	$1.6 \cdot 10^7$	$\mathcal{O}(M_{\text{CF}}L_{\text{CF}}N \log_2(L_{\text{CF}}N))$

like in [7] we use the number of RM, since a multiplication is more costly than an addition, for any hardware device or software algorithm [76, p. 320]. The proposed OSF-OPW method with $M_{\text{P}} = 10$, $M = 27$, and $M_{\text{eff}} \approx 4$ requires nearly $4L_{\text{OSF}}N + 5M_{\text{P}}N_s + 3MM_{\text{eff}} \approx 1.3 \cdot 10^5$ RM. The DVB-T2 TR method requires on average $M_{\text{TR}} \approx 6.3$ iterations and consequently costs about $M_{\text{TR}}(8L_{\text{TR}}N + 13N_s) \approx 4.2 \cdot 10^5$ RM. For ACE, we have found $M_{\text{ACE}} \approx 80.1$ and an average number of $N_{\text{d,ext}} = 1243.5$ extended points, which is similar to the estimated value $N_{\text{d}}(2\sqrt{M_{\text{qam}}} - 3)/M_{\text{qam}} \approx 1347.5$: this method is more complex and requires roughly $4L_{\text{ACE}}N \log_2(L_{\text{ACE}}N) \approx 2.0 \cdot 10^6$ RM per OFDM symbol. For CF, the complexity amounts to $4M_{\text{CF}}L_{\text{CF}}N \log_2(L_{\text{CF}}N) \approx 1.6 \cdot 10^7$ RM per OFDM symbol. Hence the RM complexity of the OSF-OPW algorithm is approximately one third of TR, roughly 15 times lower than ACE, and approximately 120 times lower than CF.

C. SIMULATED BER OF THE ADDITIONAL DATA

Fig. 9 displays the BER of the DBPSK additional data on the reserved carriers. For the theoretical evaluations, we assume

an AWGN channel, while for simulations we also consider the multipath channels: the Rician channel F1 and the NLOS channel P1 [4], [71]. As shown in the legend of Fig. 9, we also considered approaches that use a fixed number N_{h} of helpful carriers, which are those with lower projections. As shown in Fig. 9, the best BER performance is obtained by using all the N_s carriers, but in this case there is no PAPR reduction. The OSF-based PAPR reduction strategies null some reserved carriers and hence reduce the repetition factor of the DBPSK coded bit. Anyway, the BER performance is still good: thanks to repetition coding, the CNR Γ required for a BER of 10^{-4} is below 3.5 dB and hence is significantly lower than the CNR $\Gamma > 15$ dB required for the correct detection of 64-QAM data with code rate $R_c = 3/4$ [71]. For OSF-SPW with $N_{\text{h}} = N_s/2$, there is some difference between the theoretical curve (22) and the simulations, because in the simulations the selected N_{h} carriers randomly change from one OFDM symbol to the next OFDM symbol of DBPSK: therefore, those carriers that are helpful in both OFDM symbols are no longer exactly $N_{\text{h}}/2 = N_s/4$, as assumed in (22); i.e., for OSF-SPW with $N_{\text{h}} = N_s/2$, the effective repetition factor

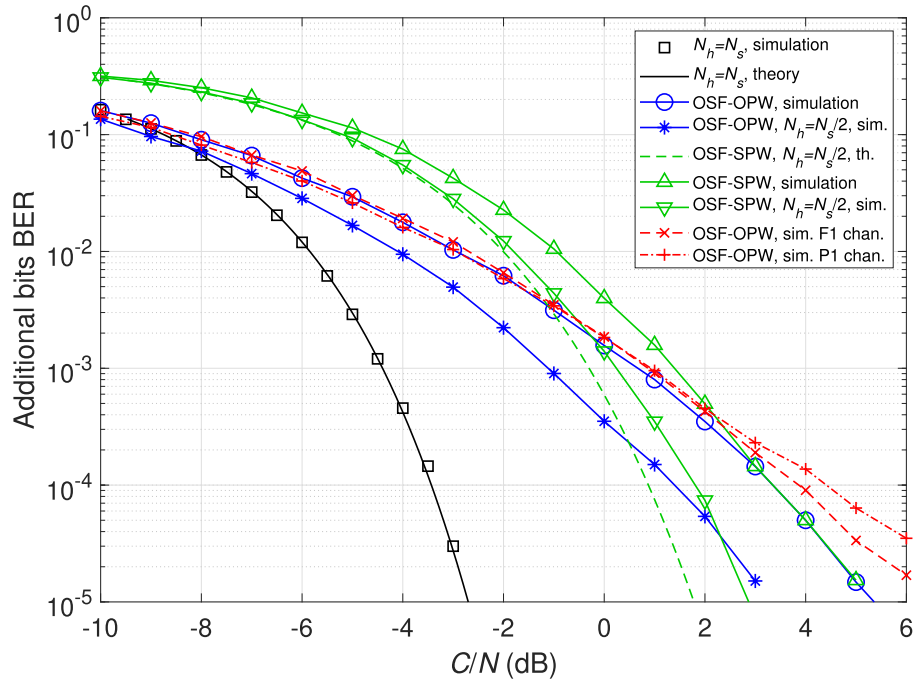


FIGURE 9. BER of the additional data carriers. When not specified in the legend, the channel model is AWGN.

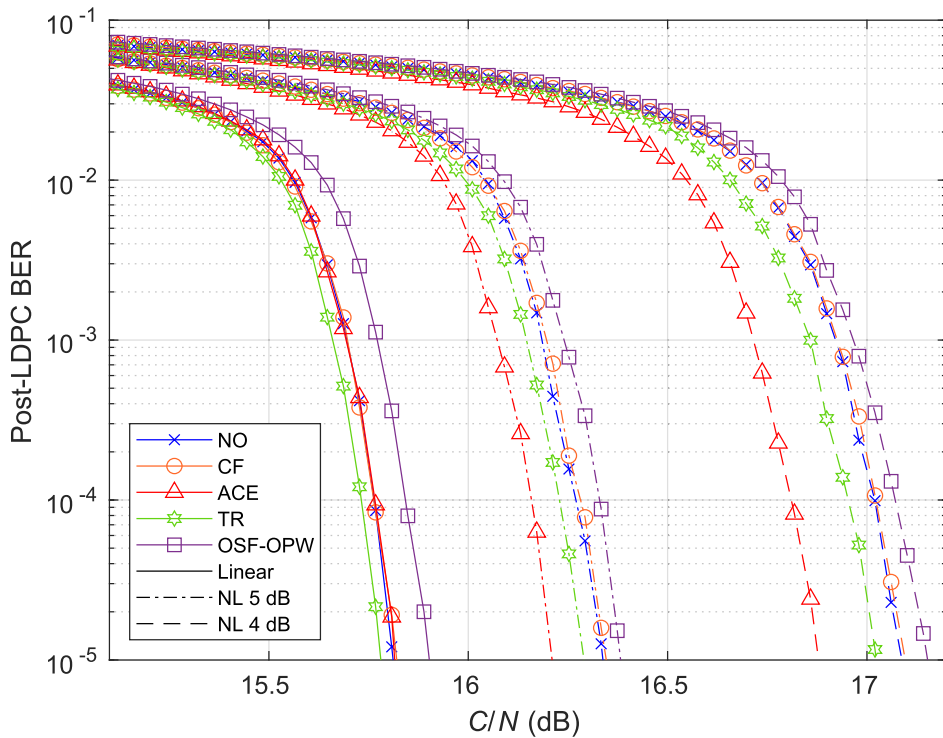


FIGURE 10. Simulated BER for the QAM data with the tested DVB-T2 PAPR reduction methods.

is a random variable, with mean $N_h/2$ but with variance larger than zero, differently from (22). In multipath channels, the BER for OSF-OPW is close to the BER in the AWGN channel: this is due to the large diversity order (around $N_s/4 = 18$) in multipath channels.

D. SIMULATED BER OF THE QAM DATA

The simulated BER of the DVB-T2 QAM data in AWGN is shown in Fig. 10, for the tested PAPR reduction methods. Both linear and nonlinear amplification is considered: the nonlinear amplifier is an ideally predistorted amplifier

operating at 4 and 5 dB of input back-off (IBO). For reference, all the simulated cases comprise also the unmodified original signal (indicated with NO in the legend of Fig. 10). The BER is estimated at the output of the LDPC decoder, assuming ideal channel knowledge, for the transmitter configuration defined before, i.e., 8K, 64-QAM, $R_c = 3/4$, and PP5 pilot pattern. The results of Fig. 10 show that, in the linear case, TR gives the best performance, followed by original, ACE, and CF, which are practically equivalent. In this condition, the OSF-OPW method has a loss of 0.1 dB. The BER improvement of TR and loss of OSF-OPW with respect to the original can be explained by how the two methods modify the reserved carriers. Indeed, while TR modifies the reserved carriers with a correction signal that has a relative power lower than that of the data, OSF-OPW does the opposite. Thus, in total, more power is dedicated to QAM data for TR, while less power is available when using OSF-OPW. This power loss of OSF-OPW is the price to be paid for giving increased robustness to the additional data on the reserved carriers. Indeed, the comparison of Fig. 10 with Fig. 9 shows that the additional data of OSF-OPW achieve a BER of 10^{-5} when the SNR is about 5.5 dB, while the QAM data achieve the same BER when the SNR is larger than 15.5 dB. Therefore, the OSF-OPW method trades the energy loss (0.1 dB) on QAM data with the increased reliability of the additional data (more than 10 dB gain).

Fig. 10 also shows that, at IBO of 5 dB, ACE stands out and achieves the best performance, with TR practically keeping the same advantage with respect to original and CF. For the reasons detailed before, OSF-OPW has a power loss with respect to the original (however, lower than in the previous case). The BER improvement of ACE is due to a combination of factors. First, ACE extends the QAM points located along the border of the constellation square, strengthening these points against noise and other impairments. In other words, the ACE method improves the performance of thousands of QAM data, while OSF-OPW and TR methods act on dozens of reserved carriers only. Second, the improved PAPR reduction of ACE yields a reduced nonlinear distortion, which produces a BER improvement with respect to the other methods. In the same Fig. 10, we have also simulated 4 dB of IBO. The curves show the same performance ranking of 5 dB, with a loss for all methods due to the higher level of nonlinear noise. With respect to 5 dB of IBO, the performance advantage of ACE is more evident and we note that OSF-OPW keeps the same performance loss with respect to the original.

In summary, OSF-OPW is able to achieve a similar BER performance to that of the other methods, with an energy loss lower than 0.1 dB; it has the advantage that it can also deliver an additional signaling stream with increased reliability, which the other methods cannot.

VII. CONCLUSION

We have proposed a novel algorithm that reduces the PAPR of the DVB-T2 signal by insertion of a coded DBPSK sequence

on the reserved carriers. The proposed OSF-OPW algorithm amplifies the reserved carriers that are helpful to reduce the PAPR, while zeroing the reserved carriers that would increase the PAPR. The proposed algorithm achieves a PAPR reduction of about 2 dB (for the 64-QAM case) with respect to the original OFDM signal, and of about 1 dB with respect to the TR algorithm of the DVB-T2 standard. The proposed algorithm is also 15 times less complex than ACE, which however has better PAPR performance, and 120 times less complex than CF (with MER = 57.4 dB) with similar PAPR performance. A nice feature of the proposed method is the introduction of additional signaling with respect to the TR PAPR reduction scheme of the DVB-T2 standard. Moreover, we highlight that the proposed PAPR reduction method is fully backward-compatible with all receivers compliant with the DVB-T and DVB-T2 standards. The proposed method could be extended to generic OFDM systems with reserved carriers by optimizing the number of reserved carriers and their position.

APPENDIX A OPTIMAL WEIGHT SEARCH ALGORITHM

We want to minimize the metric $J(W, \hat{\mathcal{H}}_O)$ in (11). To this purpose, we first rewrite every element inside the maximum in (11) as

$$\begin{aligned} |\bar{s}_m + Wh_m(\hat{\mathcal{H}}_O)|^2 &= W^2 |h_m(\hat{\mathcal{H}}_O)|^2 \\ &\quad + 2W \operatorname{Re}[\bar{s}_m h_m^*(\hat{\mathcal{H}}_O)] + |\bar{s}_m|^2 \\ &= A_m W^2 + B_m W + C_m, \end{aligned} \quad (23)$$

which is quadratic in W . Fig. 11 shows a visual example for $M = 27$: each solid line represents one of the $M = 27$ terms in (11), i.e., a parabola expressed by (23). The maximum operator in (11) returns M_{eff} parabolic segments (in our example, $M_{\text{eff}} = 3$) intersecting at points $I_1, \dots, I_{M_{\text{eff}}-1}$. From Fig. 11, it is clear that the minimum of (11) occurs either at one of the $M_{\text{eff}} + 1$ edges of the parabolic segments, or between two edges of the parabolic segments (this second case happens when the parabolic segment contains the minimum of the parabola). The arrangement of the parabolic segments suggests a reduced-complexity strategy for the search of W that minimizes the metric (11):

- 1) given an initial value $W = W_{I_0}$, evaluate (23) and find the index $m_0 = \arg \max(A_m W_{I_0}^2 + B_m W_{I_0} + C_m)$ of the parabola with the highest value in this point. This is the first dashed segment in Fig. 11, starting from I_0 ;
- 2) find the abscissas of the intersections of this parabola with all the other $M - 1$ parabolas, expressed by $W_{\pm}^{(m_0, n)} = -[(B_{m_0} - B_n) \pm \sqrt{\Delta^{(m_0, n)}}] / [2(A_{m_0} - A_n)]$, where $\Delta^{(m_0, n)} = (B_{m_0} - B_n)^2 - 4(A_{m_0} - A_n)(C_{m_0} - C_n)$. We exclude complex solutions and solutions lower than W_{I_0} ;

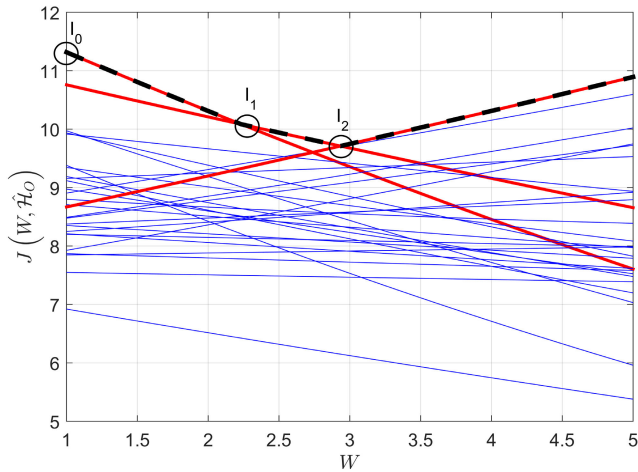


FIGURE 11. An example of the optimal weight search. The solid parabolic segments represent the terms in (23), while the dashed parabolic segments represent $J(W, \hat{H}_0)$ in (11).

- 3) choose the intersection with the lowest abscissa, corresponding to I_1 ,

$$m_1 = \arg \min_n \left(W_-^{(m_0, n)}, W_+^{(m_0, n)} \right), \quad (24)$$

$$W_{I_1} = \min_n \left(W_-^{(m_0, n)}, W_+^{(m_0, n)} \right). \quad (25)$$

This operation defines the first parabolic segment $\overline{I_0 I_1}$ in Fig. 11;

- 4) calculate the abscissa of the minimum of parabola with index m_0 given by $W_{\min}^{(m_0)} = -\frac{B_{m_0}}{2A_{m_0}}$; we exclude the solution if $W_{\min}^{(m_0)}$ is outside of the interval $[W_{I_0}, W_{I_1}]$;
- 5) switch to the intersecting parabola of index m_1 found during step 3 and repeat steps 2–4 to find the next intersection I_2 , parabola index m_2 , W_{I_2} , and $W_{\min}^{(m_1)}$;
- 6) in an iterative way, repeat step 5 for all the following segments, until the end of the search range for W is reached;
- 7) for each couple (m_n, W_{I_n}) , and for each included couple $(m_n, W_{\min}^{(m_n)})$, calculate (23) and select the optimal weight W_O that minimizes (23).

APPENDIX B DETAILS OF THE COMPUTATIONAL COMPLEXITY

In this appendix we detail the computational costs of the proposed OSF-OPW algorithm and of the alternative methods TR and ACE of [4].

The proposed OSF-OPW method requires $2LN$ RM and LN RA to find the magnitude of the signal samples and $M(LN - 1)$ VC to find the M peaks in (8); by considering the twiddle factor sequences $(K_s[i, l] + K_O)n$ precomputed and stored, the $N_s M$ contributions $s_{i,m}$ in (9) have no cost; $2N_s M$ RA to find the data-pilot contributions \bar{s}_m in (10); $2N_s M_P$ RM and $N_s M_P$ RA to find the projections $p_{i,m}$ in (16); $N_s(M_P - 1)$ RA to find the OSF in (17); $M_{\text{eff}}(3M - 2)$ RM, $4M_{\text{eff}}(M - 1)$ RA, and $4M_{\text{eff}}$ VC for (18); $8M$ RM

and $7M$ RA for (19); $M_{\text{eff}}(2M - 3)$ VC to find the lowest abscissa; $6M_{\text{eff}}$ RM and $4M_{\text{eff}}$ RA to compute the terms in (23); $2M_{\text{eff}} - 1$ VC to find the OPW weight in (20); the weighted carrier values in (6) are computed at no cost; in (21), we recall that $X_s[i, l] = \pm 1$. Then, the first term in the right hand side of (21) requires $2LN$ RM and $L(N_s/2 - 1)N$ RA, the second term also requires only $L(N_s/2 - 1)N$ RA, and the composition of the two terms requires $2LN$ further RA. Thus, this step needs $2LN$ RM and $LN_s N$ RA. In total, OSF-OPW requires $4LN + 2N_s M_P + M_{\text{eff}}(3M + 4) + 8M$ RM, $LN(N_s + 1) + N_s(2(M + M_P) - 1) + 7M + 4M_{\text{eff}}M$ RA, and $M(LN - 1) + M_{\text{eff}}(2M + 3) - 1$ VC.

About the alternative PAPR reduction methods, we consider the TR algorithm in Clause 9.6.2.1 of [4, p. 119] and the ACE algorithm in Clause 9.6.1 of [4, p. 117]. With reference to the steps 1–9 of the TR algorithm in [4, p. 119], which uses $L = L_{\text{TR}} = 1$, the cost of TR for each iteration is $2LN$ RM, LN RA, and $LN - 1$ VC for the maximum magnitude in step 2; 2 RM and 2 RA for the unit-magnitude phasor in step 3; $11N_s$ RM and $6N_s$ RA for the correction magnitude in step 4; 1 RA and $N_s + 1$ VC to find the largest magnitude of correction in step 5; $6LN$ RM and $4LN$ RA to update the peak reduction signal in step 6 (we suppose the kernels are precomputed); $2N_s$ RM and $2N_s$ RA to update the frequency domain coefficient in step 7. After the last step of the last iteration, $2LN$ RA are needed to add the peak reduction signal to the data signal. In total, the TR algorithm requires $M_{\text{TR}}(8LN + 13N_s + 2)$ RM, $2LN + M_{\text{TR}}(5LN + 8N_s + 3)$ RA, and $M_{\text{TR}}(LN + N_s)$ VC, where M_{TR} is the number of iterations.

Instead, with reference to the ACE algorithm in [4, p. 117], which uses $L = L_{\text{ACE}} = 4$, the complexity is as follows: $2LN$ RM, LN RA, and LN VC to find the position of the clipped samples of signal \mathbf{x}' in [4, p. 117]; $4M_{\text{ACE}}$ RM to find the clipped signal \mathbf{x}'' in [4, p. 117]; $2NL \log_2(NL)$ RM and $3NL \log_2(NL)$ RA for the FFT to calculate the clipped frequency signal \mathbf{X}_c in [4, p. 117]; $2N_{\text{d,ext}}$ RM and $4N_{\text{d,ext}}$ RA to obtain the combined signal \mathbf{X}'_c in [4, p. 117]. The extendable points are those on the borders of the QAM constellation: there are 4 corner points and $4(\sqrt{M_{\text{qam}}} - 2)$ side points. For equiprobable constellation points and uncorrelated clipping noise with pdf symmetrical around zero, the side points are extended with a 50% probability, whereas the corner points are extended with a 25% probability, leading to

$$\frac{N_{\text{d,ext}}}{N_{\text{d}}} \approx \frac{4(\sqrt{M_{\text{qam}}} - 2) \cdot \frac{1}{2} + 4 \cdot \frac{1}{4}}{M_{\text{qam}}} = \frac{2\sqrt{M_{\text{qam}}} - 3}{M_{\text{qam}}};$$

$4N_{\text{d,ext}}$ VC to obtain the saturated signal \mathbf{X}''_c in [4, p. 118]; $6N_{\text{d,ext}}$ VC to construct the signal \mathbf{X}_{ACE} in [4, p. 118]; an IFFT to generate the PAPR-reduced OFDM symbol with $2LN \log_2(LN)$ RM and $3LN \log_2(LN)$ RA. In total, the ACE algorithm needs $2LN(2 \log_2(LN) + 1) + 2N_{\text{d,ext}} + 4M_{\text{ACE}}$ RM, $LN(6 \log_2(LN) + 1) + 4N_{\text{d,ext}}$ RA, and $LN + 10N_{\text{d,ext}}$ VC.

APPENDIX C

THEORETICAL BER OF THE ADDITIONAL DATA

This appendix demonstrates that the bit error probability of the additional DBPSK data on the reserved carriers, using the proposed OSF approach, is equal to (22), in AWGN channels. Let us assume that the complex-valued baseband received signal on the i -th reserved carrier is expressed by $r[i, l] = W[l]\mathcal{H}[i, l]X_s[i, l] + n[i, l]$, where $l = Dq + d$ is the index of the OFDM symbol that contains $b_{q,d}$ (the q -th bit of the d -th bit sequence), $W[l]$ and $\mathcal{H}[i, l]$ are the weight and the selection function, respectively, of the PAPR reduction algorithm, $X_s[i, l]$ is the additional data expressed by (2)–(4), and $n[i, l]$ is the complex AWGN term with zero mean and variance $N_0/2$ per dimension. The DBPSK detector exploits the repetition coding and takes a decision according to the sign of the detection variable Θ_l , expressed by

$$\Theta_l = \sum_{i=0}^{N_s-1} \theta_{i,l} = \sum_{i=0}^{N_s-1} \text{Re}(r[i, l]r^*[i, l - D]). \quad (26)$$

Specifically, the estimated bit is $\hat{b}_{q,d} = 0$ when $\Theta_{Dq+d} \geq 0$, and $\hat{b}_{q,d} = 1$ when $\Theta_{Dq+d} < 0$. Without loss of generality, we assume that the transmitted bit is $b_{q,d} = 0$, which leads to $X_s[i, l - D] = X_s[i, l]$, and we evaluate the error probability as $P_b = \Pr\{\Theta_l < 0 | b_{q,d} = 0\}$. Using the approach of [77, p. 1090–1095], the error probability can be expressed by

$$P_b = -\frac{1}{2\pi j} \int_{-\infty + j\epsilon}^{+\infty + j\epsilon} \frac{\psi_{\Theta_l}(jv)}{v} dv, \quad (27)$$

where $\psi_{\Theta_l}(jv)$ is the characteristic function of the decision variable Θ_l and ϵ is a positive constant. Since the noise terms on different carriers are independent, the random variables $\{\theta_{i,l}\}_{i=0}^{N_s-1}$ in (26) are independent, and therefore $\psi_{\Theta_l}(jv) = \prod_{i=0}^{N_s-1} \psi_{\theta_{i,l}}(jv)$. The characteristic function of $\theta_{i,l}$ can be calculated as

$$\psi_{\theta_{i,l}}(jv) = \frac{(2/N_0)^2}{v^2 + (2/N_0)^2} \exp\left[\frac{(2/N_0)^2 g_{i,l}(jv)}{v^2 + (2/N_0)^2}\right], \quad (28)$$

where $g_{i,l}(jv)$ depends on the selection function $\mathcal{H}[i, l]$ and $\mathcal{H}[i, l - D]$. We have to distinguish the following four cases.

- $\mathcal{H}[i, l] = \mathcal{H}[i, l - D] = 1$, i.e., the i -th reserved carrier is helpful for PAPR reduction for both the l -th and the $(l - D)$ -th OFDM symbols: in this case, $g_{i,l}(jv) = -v^2(W^2[l] + W^2[l - D])N_0/4 + jvW[l]W[l - D]$.
- $\mathcal{H}[i, l] = \mathcal{H}[i, l - D] = 0$, i.e., the i -th reserved carrier is dangerous for PAPR reduction for both the l -th and the $(l - D)$ -th OFDM symbols: in this case, $g_{i,l}(jv) = 0$.
- $\mathcal{H}[i, l] = 1$ and $\mathcal{H}[i, l - D] = 0$, i.e., the i -th reserved carrier is helpful for the l -th OFDM symbol and dangerous for the $(l - D)$ -th OFDM symbol: in this case, $g_{i,l}(jv) = -v^2W^2[l]N_0/4$.
- $\mathcal{H}[i, l] = 0$ and $\mathcal{H}[i, l - D] = 1$, i.e., the i -th reserved carrier is dangerous for the l -th OFDM symbol and helpful for the $(l - D)$ -th OFDM symbol: in this case, $g_{i,l}(jv) = -v^2W^2[l - D]N_0/4$.

On average, each case happens for $N_s/4$ reserved carriers. By assuming that the received energy is constant (i.e., $W[l] = W[l - D] = \sqrt{E_b}$), and combining all the equations, $\psi_{\Theta_l}(jv)$ becomes

$$\psi_{\Theta_l}(jv) = \left[\frac{(2/N_0)^2}{v^2 + (2/N_0)^2} \right]^{N_s} \exp\left[\frac{(2/N_0)^2 G(jv)}{v^2 + (2/N_0)^2}\right], \quad (29)$$

where $G(jv) = \sum_{i=0}^{N_s-1} g_{i,l}(jv) = -v^2N_sE_bN_0/4 + jvN_sE_b/4$. Equations (27) and (29) have the same form of [77, p. 1091, eq. (B-4)] and [77, p. 1091, eq. (B-7)], respectively. Consequently, the error probability is expressed by [77, p. 1094, eq. (B-21)]

$$P_b = Q_1\left(\sqrt{\frac{1}{4}N_s\gamma}, \sqrt{\frac{3}{4}N_s\gamma}\right) - e^{-\frac{N_s\gamma}{2}} I_0\left(\frac{\sqrt{3}}{4}N_s\gamma\right) + \frac{1}{2^{2N_s-1}} e^{-\frac{N_s\gamma}{2}} I_0\left(\frac{\sqrt{3}}{4}N_s\gamma\right) \sum_{i=0}^{N_s-1} \binom{2N_s-1}{i} + \frac{e^{-\frac{N_s\gamma}{2}}}{2^{2N_s-1}} \sum_{n=1}^{N_s-1} I_n\left(\frac{\sqrt{3}}{4}N_s\gamma\right) \sum_{k=0}^{N_s-1-n} \binom{2N_s-1}{k} (3^{\frac{n}{2}} - 3^{-\frac{n}{2}}), \quad (30)$$

where $Q_1(\cdot, \cdot)$ is the Marcum Q function of first order, $I_n(\cdot)$ is the modified Bessel function of the first kind and order n , $\gamma = E_b/N_0$ is the SNR on the reserved carriers. Equation (22) is obtained from (30) by exploiting

$$\sum_{i=0}^{N_s-1} \binom{2N_s-1}{i} = 2^{2N_s-2}, \quad (31)$$

$$3^{\frac{n}{2}} - 3^{-\frac{n}{2}} = 2 \sinh\left(\frac{n \log_e 3}{2}\right). \quad (32)$$

REFERENCES

- [1] L. Dai, Z. Wang, and Z. Yang, "Next-generation digital television terrestrial broadcasting systems: Key technologies and research trends," *IEEE Commun. Mag.*, vol. 50, no. 6, pp. 150–158, Jun. 2012.
- [2] K. Weber, "4K, HDR and further image enhancements for live image acquisition," in *Proc. SMPTE Annu. Tech. Conf. Exhib.*, Hollywood, CA, USA, Oct. 2015, pp. 1–21.
- [3] J. Yurek, "Ultra high definition: Beyond pixel count," *IEEE Consum. Electron. Mag.*, vol. 4, no. 4, pp. 89–91, Oct. 2015.
- [4] *DVB; Frame Structure Channel Coding and Modulation for a Second Generation Digital Terrestrial Television Broadcasting System (DVB-T2)*, document ETSI EN 302 755, V1.4.1, Jul. 2015.
- [5] S. C. Thompson, J. G. Proakis, and J. R. Zeidler, "The effectiveness of signal clipping for PAPR and total degradation reduction in OFDM systems," in *Proc. IEEE Global Telecommun. Conf. (GLOBECOM)*, St. Louis, MO, USA, Dec. 2005, pp. 2807–2811.
- [6] T. Jiang and Y. Wu, "An overview: Peak-to-average power ratio reduction techniques for OFDM signals," *IEEE Trans. Broadcast.*, vol. 54, no. 2, pp. 257–268, Jun. 2008.
- [7] Y. Rahmatallah and S. Mohan, "Peak-to-average power ratio reduction in OFDM systems: A survey and taxonomy," *IEEE Commun. Surveys Tuts.*, vol. 15, no. 4, pp. 1567–1592, 4th Quart., 2013.
- [8] J. Armstrong, "Peak-to-average power reduction for OFDM by repeated clipping and frequency domain filtering," *Electron. Lett.*, vol. 38, no. 5, pp. 246–247, Feb. 2002.
- [9] Y.-C. Wang and Z.-Q. Luo, "Optimized iterative clipping and filtering for PAPR reduction of OFDM signals," *IEEE Trans. Commun.*, vol. 59, no. 1, pp. 33–37, Jan. 2011.
- [10] S. Gökceli, T. Levanen, T. Riihonen, J. Yli-Kaakinen, A. Brihuega, M. Turunen, M. Renfors, and M. Valkama, "Novel iterative clipping and error filtering methods for efficient PAPR reduction in 5G and beyond," *IEEE Open J. Commun. Soc.*, vol. 2, pp. 48–66, 2021.

- [11] A. M. Rateb and M. Labana, "An optimal low complexity PAPR reduction technique for next generation OFDM systems," *IEEE Access*, vol. 7, pp. 16406–16420, 2019.
- [12] T. Jiang, Y. Yang, and Y.-H. Song, "Exponential companding technique for PAPR reduction in OFDM systems," *IEEE Trans. Broadcast.*, vol. 51, no. 2, pp. 244–248, Jun. 2005.
- [13] Y. Jiang, "New companding transform for PAPR reduction in OFDM," *IEEE Commun. Lett.*, vol. 14, no. 4, pp. 282–284, Apr. 2010.
- [14] A. Goel, P. G. Poddar, and M. Agrawal, "A novel quadrilateral companding transform for PAPR reduction in OFDM systems," *Digit. Signal Process.*, vol. 85, pp. 113–123, Feb. 2019.
- [15] Z. Xing, K. Liu, A. S. Rajasekaran, H. Yanikomeroğlu, and Y. Liu, "A hybrid companding and clipping scheme for PAPR reduction in OFDM systems," *IEEE Access*, vol. 9, pp. 61565–61576, 2021.
- [16] M. Al-Gharabally, A. F. Almutairi, and A. Krishna, "Performance analysis of the two-piecewise linear companding technique on filtered-OFDM systems," *IEEE Access*, vol. 9, pp. 48793–48802, 2021.
- [17] A. Mohammed, T. Ismail, A. Nassar, and H. Mostafa, "A novel companding technique to reduce high peak to average power ratio in OFDM systems," *IEEE Access*, vol. 9, pp. 35217–35228, 2021.
- [18] M. Hu, Y. Li, W. Wang, and H. Zhang, "A piecewise linear companding transform for PAPR reduction of OFDM signals with companding distortion mitigation," *IEEE Trans. Broadcast.*, vol. 60, no. 3, pp. 532–539, Sep. 2014.
- [19] T. Jiang, C. Ni, and Y. Xu, "Novel 16-QAM and 64-QAM near-complementary sequences with low PMEPR in OFDM systems," *IEEE Trans. Commun.*, vol. 64, no. 10, pp. 4320–4330, Oct. 2016.
- [20] Y. Wang, M. Wang, and Z. Xie, "A PAPR reduction method with EVM constraints for OFDM systems," *IEEE Access*, vol. 7, pp. 171830–171839, 2019.
- [21] Y. Huang, S. Hu, S. Ma, Z. Liu, and M. Xiao, "Designing low-PAPR waveform for OFDM-based RadCom systems," *IEEE Trans. Wireless Commun.*, vol. 21, no. 9, pp. 6979–6993, Sep. 2022.
- [22] Y. Huleihel, E. Ben-Dror, and H. H. Permuter, "Low PAPR waveform design for OFDM systems based on convolutional autoencoder," in *Proc. IEEE Int. Conf. Adv. Netw. Telecommun. Syst. (ANTS)*, New Delhi, India, Dec. 2020, pp. 1–6.
- [23] S. H. Han and J. H. Lee, "An overview of peak-to-average power ratio reduction techniques for multicarrier transmission," *IEEE Wireless Commun.*, vol. 12, no. 2, pp. 56–65, Apr. 2005.
- [24] D. Bi, P. Ren, and Z. Xiang, "A novel joint PAPR reduction algorithm with low complexity using LT codes," *IEEE Wireless Commun. Lett.*, vol. 7, no. 2, pp. 166–169, Apr. 2018.
- [25] T. Matsumine and H. Ochiai, "A novel PAPR reduction scheme for polar-coded OFDM systems," *IEEE Commun. Lett.*, vol. 23, no. 12, pp. 2372–2375, Dec. 2019.
- [26] S. Nihei, M. Umehira, and S. Takeda, "A modified DFTs-OFDM with DC subcarrier shift for low PAPR and DC offset error robustness," in *Proc. IEEE 81st Veh. Technol. Conf. (VTC Spring)*, Glasgow, U.K., May 2015, pp. 1–6.
- [27] D. Kong, X. Zheng, Y. Yang, Y. Zhang, and T. Jiang, "A novel DFT-based scheme for PAPR reduction in FBMC/OQAM systems," *IEEE Wireless Commun. Lett.*, vol. 10, no. 1, pp. 161–165, Jan. 2021.
- [28] M. Park, H. Jun, J. Cho, N. Cho, D. Hong, and C. Kang, "PAPR reduction in OFDM transmission using Hadamard transform," in *Proc. IEEE Internat. Conf. Commun.*, vol. 1, New Orleans, LA, USA, Jun. 2000, pp. 430–433.
- [29] T. Arbi, Z. Ye, and B. Geller, "Low-complexity blind PAPR reduction for OFDM systems with rotated constellations," *IEEE Trans. Broadcast.*, vol. 67, no. 2, pp. 491–499, Jun. 2021.
- [30] J. Zheng and H. Lv, "Peak-to-average power ratio reduction in OFDM index modulation through convex programming," *IEEE Commun. Lett.*, vol. 21, no. 7, pp. 1505–1508, Jul. 2017.
- [31] M. Kim, W. Lee, and D.-H. Cho, "A novel PAPR reduction scheme for OFDM system based on deep learning," *IEEE Commun. Lett.*, vol. 22, no. 3, pp. 510–513, Mar. 2018.
- [32] S. Lv, J. Zhao, L. Yang, and Q. Li, "Genetic algorithm based bilayer PTS scheme for peak-to-average power ratio reduction of FBMC/OQAM signal," *IEEE Access*, vol. 8, pp. 17945–17955, 2020.
- [33] S. Yoo, S. Yoon, S. Yong Kim, and I. Song, "A novel PAPR reduction scheme for OFDM systems: Selective mapping of partial tones (SMOPT)," *IEEE Trans. Consum. Electron.*, vol. 52, no. 1, pp. 40–43, Feb. 2006.
- [34] T. Jiang, W. Xiang, P. C. Richardson, J. Guo, and G. Zhu, "PAPR reduction of OFDM signals using partial transmit sequences with low computational complexity," *IEEE Trans. Broadcast.*, vol. 53, no. 3, pp. 719–724, Sep. 2007.
- [35] E. Al-Dalakta, A. Al-Dweik, A. Hazmi, C. Tsimenidis, and B. Sharif, "PAPR reduction scheme using maximum cross correlation," *IEEE Commun. Lett.*, vol. 16, no. 12, pp. 2032–2035, Dec. 2012.
- [36] C. Ye, Z. Li, T. Jiang, C. Ni, and Q. Qi, "PAPR reduction of OQAM-OFDM signals using segmental PTS scheme with low complexity," *IEEE Trans. Broadcast.*, vol. 60, no. 1, pp. 141–147, Mar. 2014.
- [37] K.-S. Lee, H. Kang, and J.-S. No, "New PTS schemes with adaptive selection methods of dominant time-domain samples in OFDM systems," *IEEE Trans. Broadcast.*, vol. 64, no. 3, pp. 747–761, Sep. 2018.
- [38] Z. He, L. Zhou, Y. Chen, and X. Ling, "Low-complexity PTS scheme for PAPR reduction in FBMC-OQAM systems," *IEEE Commun. Lett.*, vol. 22, no. 11, pp. 2322–2325, Nov. 2018.
- [39] L. J. Cimini and N. R. Sollenberger, "Peak-to-average power ratio reduction of an OFDM signal using partial transmit sequences with embedded side information," in *Proc. IEEE Global Telecommun. Conf.*, vol. 2, San Francisco, CA, USA, Nov. 2000, pp. 746–750.
- [40] S. H. Han and J. H. Lee, "Modified selected mapping technique for PAPR reduction of coded OFDM signal," *IEEE Trans. Broadcast.*, vol. 50, no. 3, pp. 335–341, Sep. 2004.
- [41] K.-H. Kim, "On the phase sequences and permutation functions in the SLM scheme for OFDM-IM systems," *IEEE Access*, vol. 8, pp. 121733–121743, 2020.
- [42] M. S. Hossain and T. Shimamura, "Low-complexity null subcarrier-assisted OFDM PAPR reduction with improved BER," *IEEE Commun. Lett.*, vol. 20, no. 11, pp. 2249–2252, Nov. 2016.
- [43] Y. Wang, Y. Wang, and Q. Shi, "Optimized signal distortion for PAPR reduction of OFDM signals with IFFT/FFT complexity via ADMM approaches," *IEEE Trans. Signal Process.*, vol. 67, no. 2, pp. 399–414, Jan. 2019.
- [44] J. Tellado, "Peak-to-average power reduction for multicarrier modulation," Ph.D. dissertation, Dept. Elect. Eng., Stanford Univ., Stanford, CA, USA, 1999.
- [45] M. Mroué, A. Nafkha, J. Palicot, B. Gavalda, and N. Dagherne, "Performance and implementation evaluation of TR PAPR reduction methods for DVB-T2," *Int. J. Digit. Multimedia Broadcast.*, vol. 2010, Aug. 2010, Art. no. 797393.
- [46] S. S. K. C. Bulusu, M. Crussière, J.-F. Hélar, R. Mounzer, Y. Nasser, O. Rousset, and A. Untersee, "Quasi-optimal tone reservation PAPR reduction algorithm for next generation broadcasting systems: A performance/complexity/latency tradeoff with testbed implementation," *IEEE Trans. Broadcast.*, vol. 64, no. 4, pp. 883–899, Dec. 2018.
- [47] N. Lahbabi, S. S. K. C. Bulusu, J.-F. Hélar, and M. Crussière, "Very efficient tone reservation PAPR reduction fully compatible with ATSC 3.0 standard: Performance and practical implementation analysis," *IEEE Access*, vol. 6, pp. 58355–58372, 2018.
- [48] H. Li, T. Jiang, and Y. Zhou, "An improved tone reservation scheme with fast convergence for PAPR reduction in OFDM systems," *IEEE Trans. Broadcast.*, vol. 57, no. 4, pp. 902–906, Dec. 2011.
- [49] Y. Wang, S. Xie, and Z. Xie, "FISTA-based PAPR reduction method for tone reservation's OFDM system," *IEEE Wireless Commun. Lett.*, vol. 7, no. 3, pp. 300–303, Jun. 2018.
- [50] M. E. Hassan, M. Crussière, J.-F. Hélar, Y. Nasser, and O. Bazzi, "Theoretical performance of the gradient-based tone reservation PAPR reduction algorithm," in *Proc. 16th Int. Conf. Wireless Mobile Comput., Netw. Commun. (WiMob)*, Thessaloniki, Greece, Oct. 2020, pp. 1–6.
- [51] M. El Hassan, M. Crussière, J.-F. Hélar, Y. Nasser, and O. Bazzi, "EVM closed-form expression for OFDM signals with tone reservation-based PAPR reduction," *IEEE Trans. Wireless Commun.*, vol. 19, no. 4, pp. 2352–2366, Apr. 2020.
- [52] M. ElHassan, M. Crussière, J.-F. Hélar, Y. Nasser, and O. Bazzi, "On providing the theoretical EVM limit for tone reservation PAPR reduction technique," in *Proc. IEEE 21st Int. Workshop Signal Process. Adv. Wireless Commun. (SPAWC)*, Atlanta, GA, USA, May 2020, pp. 1–5.
- [53] Z. Liu, W. Liu, L. Hu, L. Zhang, and F. Yang, "A low complexity improved tone reservation method based on ADMM for OFDM systems' PAPR reduction," in *Proc. 13th Int. Conf. Wireless Commun. Signal Process. (WCSP)*, Changsha, China, Oct. 2021, pp. 1–5.

- [54] R. Mounzer, Y. Nasser, M. Crussière, and J.-F. Héland, "Power control optimization for tone reservation based PAPR reduction algorithms," in *Proc. IEEE 25th Annu. Int. Symp. Pers., Indoor, Mobile Radio Commun. (PIMRC)*, Washington, DC, USA, Sep. 2014, pp. 97–102.
- [55] T. Jiang, C. Ni, C. Ye, Y. Wu, and K. Luo, "A novel multi-block tone reservation scheme for PAPR reduction in OQAM-OFDM systems," *IEEE Trans. Broadcast.*, vol. 61, no. 4, pp. 717–722, Dec. 2015.
- [56] R. Zayani, H. Šaiček, and D. Roviras, "Ping-pong joint optimization of PAPR reduction and HPA linearization in OFDM systems," *IEEE Trans. Broadcast.*, vol. 65, no. 2, pp. 308–315, Jun. 2019.
- [57] Q. Nguyen, T. K. Nguyen, H. H. Nguyen, and B. Berscheid, "Novel PAPR reduction algorithms for OFDM signals," *IEEE Access*, vol. 10, pp. 77452–77461, 2022.
- [58] A. Shehata, P. Mary, and M. Crussiere, "Analysis of compressing PAPR-reduced OFDM IQ samples for cloud radio access network," *IEEE Trans. Broadcast.*, vol. 68, no. 3, pp. 765–779, Sep. 2022.
- [59] W. Wu, Y. Cao, S. Wang, and Y. Wang, "Joint optimization of PAPR reduction based on modified TR scheme for MIMO-OFDM radar," *Digit. Signal Process.*, vol. 80, pp. 27–36, Sep. 2018.
- [60] B. S. Krongold and D. L. Jones, "PAR reduction in OFDM via active constellation extension," *IEEE Trans. Broadcast.*, vol. 49, no. 3, pp. 258–268, Sep. 2003.
- [61] Z. Zheng and G. Li, "An efficient FPGA design and performance testing of the ACE algorithm for PAPR reduction in DVB-T2 systems," *IEEE Trans. Broadcast.*, vol. 63, no. 1, pp. 134–143, Mar. 2017.
- [62] Y. Kou, W.-S. Lu, and A. Antoniou, "A new peak-to-average power-ratio reduction algorithm for OFDM systems via constellation extension," *IEEE Trans. Wireless Commun.*, vol. 6, no. 5, pp. 1823–1832, May 2007.
- [63] M. Zhang, M. Liu, and Z. Zhong, "Neural network assisted active constellation extension for PAPR reduction of OFDM system," in *Proc. 11th Int. Conf. Wireless Commun. Signal Process. (WCSP)*, Xi'an, China, Oct. 2019, pp. 1–6.
- [64] R. J. Barsanti and J. Larue, "Peak to average power ratio reduction for digital video broadcast T2," in *Proc. IEEE Southeastcon*, Nashville, TN, USA, Mar. 2011, pp. 117–121.
- [65] L. Fay, L. Michael, D. Gómez-Barquero, N. Ammar, and M. W. Caldwell, "An overview of the ATSC 3.0 physical layer specification," *IEEE Trans. Broadcast.*, vol. 62, no. 1, pp. 159–171, Mar. 2016.
- [66] B. Tang, K. Qin, and H. Mei, "A hybrid approach to reduce the PAPR of OFDM signals using clipping and companding," *IEEE Access*, vol. 8, pp. 18984–18994, 2020.
- [67] S.-Y. Zhang and B. Shahrrava, "A hybrid PAPR reduction scheme for OFDM systems using perfect sequences," *IEEE Trans. Broadcast.*, vol. 66, no. 1, pp. 177–186, Mar. 2020.
- [68] J. Palicot, Y. Louet, and D. Cuel, "Tone reservation based Gaussian clipping and filtering for OFDM PAPR mitigation," in *Proc. 25th Int. Conf. Telecommun. (ICT)*, Saint-Malo, France, Jun. 2018, pp. 593–599.
- [69] S. Thota, Y. Kamatham, and C. S. Paidimarry, "Analysis of hybrid PAPR reduction methods of OFDM signal for HPA models in wireless communications," *IEEE Access*, vol. 8, pp. 22780–22791, 2020.
- [70] K. Tahkoubit, A. Ali-Pacha, H. Šaiček, and D. Roviras, "Iterative dichotomy PAPR reduction method for multicarrier waveforms," *IEEE Commun. Lett.*, vol. 23, no. 11, pp. 2073–2076, Nov. 2019.
- [71] *Digital Video Broadcasting (DVB); Implementation Guidelines for a Second Generation Digital Terrestrial Television Broadcasting System (DVB-T2)*, document ETSI TS 102 831, V1.2.1, Aug. 2012.
- [72] *DVB; Framing Structure, Channel Coding and Modulation for Digital Terrestrial Television*, document ETSI EN 300 744, V1.6.1, Jan. 2009.
- [73] G. Baruffa, L. Rugini, F. Frescura, and P. Banelli, "Real-time generation of standard-compliant DVB-T signals," *Radioengineering*, vol. 27, no. 2, pp. 475–484, Jun. 2018.
- [74] V. Savaux and Y. Louët, "PAPR analysis as a ratio of two random variables: Application to multicarrier systems with low subcarriers number," *IEEE Trans. Commun.*, vol. 66, no. 11, pp. 5732–5739, Nov. 2018.
- [75] M. Tariq, A. Al-Dweik, B. Mohammad, H. Saleh, and T. Stouraitis, "Computational power evaluation for energy-constrained wireless communications systems," *IEEE Open J. Commun. Soc.*, vol. 1, pp. 308–319, 2020.
- [76] D. E. Knuth, *The Art of Computer Programming*, vol. 2, 3rd ed. Reading, MA, USA: Addison-Wesley, 1997.
- [77] J. G. Proakis and M. Salehi, *Digital Communications*, 5th ed. Boston, MA, USA: McGraw-Hill, 2008.

GIUSEPPE BARUFFA was born in Perugia, Italy, in 1970. He received the Laurea degree in electronic engineering and the Ph.D. degree in telecommunications engineering from the University of Perugia, Perugia, in 1996 and 2001, respectively. In 2005, he visited the Swiss Federal Polytechnic of Lausanne, Lausanne, Switzerland. Since 2005, he has been an Assistant Professor with the Department of Engineering, University of Perugia. His main research interests include digital television broadcasting, joint source/channel video coding, and LPWAN sensor networks.

LUCA RUGINI (Member, IEEE) was born in Perugia, Italy, in 1975. He received the Laurea degree (cum laude) in electronic engineering and the Ph.D. degree in telecommunications engineering from the University of Perugia, Perugia, in 2000 and 2003, respectively. In 2007, he visited the Delft University of Technology, Delft, The Netherlands. He is currently an Assistant Professor with the Department of Engineering, University of Perugia. His research interest includes signal processing for communications. He has been serving as an Area Editor for *Digital Signal Processing*, since 2023. He has served as an Associate Editor for the IEEE SIGNAL PROCESSING LETTERS, from 2014 to 2018, the *Digital Signal Processing*, from 2012 to 2022, and the *EURASIP Journal on Advances in Signal Processing*, from 2015 to 2022.

FABRIZIO FRESCURA received the Laurea degree (cum laude) in electronic engineering and the Ph.D. degree in telecommunications engineering from the University of Perugia, in 1992 and 1997, respectively. Since January 2005, he has been an Assistant Professor with the Department of Engineering, University of Perugia, where he is currently a Lecturer of digital signal processing courses. He was an "Advising Professor" of the Winning Team of the "Texas Instruments 1997 DSP Solution Challenge." From 1999 to 2000, he was with Texas Instruments France. In 2000, he was the Co-Founder of the university spin-off company Digilab2000. Since 2001, he coordinates the research activity with the DSP Laboratory, University of Perugia. His research interests include DSP for image/video processing and transmission, and DSP implementation.

PAOLO BANELLI (Member, IEEE) received the Laurea degree (cum laude) in electronics engineering and the Ph.D. degree in telecommunications engineering from the University of Perugia, Perugia, Italy, in 1993 and 1998, respectively. He was a Visiting Researcher with the University of Minnesota, Minneapolis, MN, USA, in 2001, and a Visiting Professor with Stony Brook University, Stony Brook, NY, USA, from 2019 to 2020. Since 2019, he has been a Full Professor with the Department of Engineering, University of Perugia, where he has been an Associate Professor, since 2005, and an Assistant Professor, since 1998. His research interests include signal processing and optimization for wireless communications, graph signal processing and learning, and signal processing for biomedical applications. He was a member of the IEEE Signal Processing for Communications and Networking Technical Committee, from 2011 to 2013. In 2009, he was the General Co-Chair of the IEEE International Symposium on Signal Processing Advances for Wireless Communications. He served as an Associate Editor for the IEEE TRANSACTIONS ON SIGNAL PROCESSING, from 2013 to 2016. He has been serving as an Associate Editor for the *EURASIP Journal on Advances in Signal Processing*, since 2013, and IEEE OPEN JOURNAL OF SIGNAL PROCESSING, since 2020.